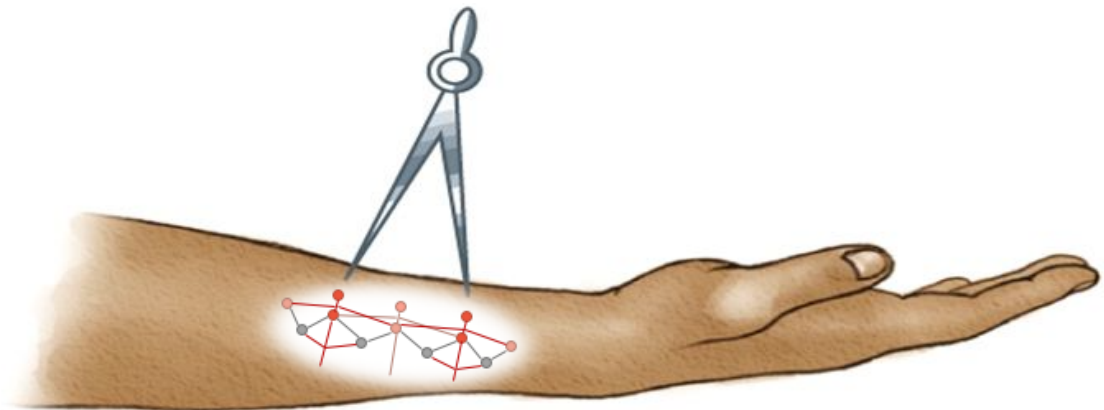




AALBORG UNIVERSITY
DENMARK

Modeling Lateral Inhibition



Master's Thesis
Aalborg University
Biomedical Engineering & Informatics
Spring 2018
Group 10405

Barak El-Omar
Navinder Singh Dhillon

Title:

Modeling Lateral Inhibition

Theme:

Master's thesis

Project Period:

Spring Semester 2018

Project Group:

Group 10405

Participant(s):

Barak El-Omar

Navinder Singh Dhillon

Supervisor(s):

Main-supervisor: Steffen Frahm

CO-supervisor: Carsten Dahl Mørch

Page Numbers: 79

Date of Completion:

07/06-2018

Abstract:

Lateral inhibition is characterized by sharpening of a sensory sensation and plays a crucial role in discrimination of sensory input. [Strominger et al., 2012] One aspect of lateral inhibition is that localization of stimuli has shown to be more difficult for noxious stimuli compared to innocuous stimuli [Quevedo et al., 2017; Frahm et al., 2017]. In order to investigate the discriminatory differences between noxious and innocuous stimuli a single-layer artificial neural network was developed and trained in MATLAB R2017b (MathWorks inc.) modelling lateral inhibition for both noxious and innocuous stimuli. The model was trained using the Gradient descent method with two-point discrimination data acquired from Frahm et al. [2017]. A validation of the lateral inhibition model for laser stimulation showed that it was able to fit the training data with a prediction error of 0.0102 mm. However, the model was not able to generalize solutions compared to the lateral inhibition model for mechanical stimulation. The reason being the lateral inhibition model for mechanical stimulation had a prediction error of 0.0618 mm and therefore not fitted to the training data to the same extent as for laser stimulation. This resulted in the lateral inhibition model for mechanical stimulation being able to poorly generalize solutions. Designing, implementing and validating a lateral inhibition model for laser and mechanical stimulation to investigate the discriminatory differences between both modalities was accomplished.

Preface

The present report is the product of the Master's thesis at the 4th semester MSc in Biomedical Engineering & Informatics. It was produced by Barak El-Omar and Navinder Singh Dhillon of group 10405, at the Department of Health Science and Technology, Aalborg University, spring 2018. The master thesis has been supervised by Steffen Frahm and Carsten Dahl Mørch.

Reading instruction

Citation was done using the Harvard method as [author's last name, publication year]. The citation for a particular sentence is done by placing the citation before a period, and after a period for the citation of a section.

Table of Contents

| | | |
|------------------|--|-----------|
| Chapter 1 | Introduction | 1 |
| Chapter 2 | Problem Analysis | 3 |
| 2.1 | Cutaneous sensory neurons | 3 |
| 2.2 | Lateral inhibition | 6 |
| 2.3 | Artificial neural network model development | 11 |
| 2.4 | Summary | 15 |
| 2.5 | Problem statement | 16 |
| Chapter 3 | Methodology | 17 |
| 3.1 | Data acquisition | 17 |
| 3.2 | Model overview | 18 |
| 3.3 | Lateral inhibition model | 18 |
| 3.4 | Model training | 26 |
| 3.5 | Data analysis | 36 |
| 3.6 | Sensitivity analysis | 36 |
| 3.7 | Model validation | 37 |
| Chapter 4 | Results | 39 |
| 4.1 | Model output | 39 |
| 4.2 | Sensitivity analysis | 48 |
| 4.3 | Model validation | 50 |
| Chapter 5 | Discussion | 53 |
| Chapter 6 | Conclusion | 59 |
| | Bibliography | 61 |
| | Appendix A Sensory pathways | 65 |
| | Appendix B Experimental procedure | 67 |
| | Appendix C Self-organizing neural networks | 69 |
| | Appendix D Results for lateral inhibition model for laser stimulation | 73 |
| | Appendix E Previous model designs | 77 |

Introduction

1

The sensory nervous system of humans has been the subject of research throughout history, and will likely continue for many years ahead. In order to investigate how the sensory nervous system functions, different research techniques such as psychophysical or electrophysical techniques have been applied. While much of the sensory nervous system is well understood and the research on the sensory nervous system is extensive, there are areas in which current knowledge is not insufficient and further research must therefore be conducted.

Part of the sensory nervous system that has been of interest is the somatosensory nervous system, that functions to respond to changes occurring on the surface or inner parts of the body. Research of the somatosensory system have often focused on stimulation of cutaneous tissues, which is due to it being more accessible, non-invasive and easier to stimulate.

The somatosensory nervous system consists of various sensory neurons that are activated during stimulation of their receptive field which is an area, that when stimulated causes activation of a sensory neuron for that specific field [Kandel et al., 2013]. The sensory neurons respond to various modalities of noxious or innocuous stimuli, such as mechanoreceptors that respond to mechanical stimuli, thermal receptors that respond to temperature changes, chemoreceptors that respond to changes in chemical concentrations and nociceptors which respond to any noxious stimuli. The afferent input on the nociceptor travels through the spinothalamic tract, while that of innocuous stimuli travels through dorsal column pathway thus transducing sensory information differently in the spinal cord before relaying the information to the higher centers of the brain. [Martini et al., 2015; Kandel et al., 2013; Feher, 2017]

A large part of the research related to the somatosensory system has focused on the concept of neural inhibition, which in general functions to regulate the behavior of excitation. More specifically there has been an interest in lateral inhibition which is characterized by sharpening of a sensory sensation and localizing stimuli. [Strominger et al., 2012] Lateral inhibition exists for all senses and plays a crucial role in discrimination of sensory input. Literature regarding lateral inhibition is extensive in relation to vision [Sirosh and Miikkulainen, 1993; Hennig et al., 2008], but it has also shown to be involved in the two-point discrimination threshold, which is the threshold where one can reliably distinguish two points from a single point [McGee, 2018].

Several factors influences related to lateral inhibition in the somatosensory system affects the capability to localize a single stimulation point and distinguish two points and are important to consider. Some of these are related to modality, stimulation size, receptive

field size, intensity etc. An interesting aspect of lateral inhibition is that localization of stimuli has shown to be more difficult for noxious stimuli compared to innocuous stimuli. [Quevedo et al., 2017; Frahm et al., 2017] However, it not clearly understood why this difference occurs due lack of knowledge about lateral inhibition. It has been suggested that the lateral inhibition mechanisms of pain-patients are diminished compared to healthy people, which may be related to the lower spatial acuity found for noxious stimuli. [Quevedo et al., 2017] Therefore it could be considered of interest to further investigate the differences in lateral inhibition between noxious and innocuous stimuli, and while some of the mechanisms involved in lateral inhibition are relatively well understood, the current knowledge is not sufficient to determine what actually happens at a deeper level.

Therefore, development of a mathematical model is feasible in order to describe or characterize specifically where the differences lie and why they occur. Modelling techniques such as Artificial Neural Networks has previously been successfully applied to model lateral inhibition in vision [Sirosh and Miikkulainen, 1993]. However, the networks implemented have typically been fully connected multi-layer networks, which are not suitable when trying to understand the exact biological mechanisms that occur in a lateral inhibition system.

Problem Analysis 2

Lateral inhibition is characterized by sharpening sensory sensations and enhancing localization of stimuli. In the context of stimulating cutaneous sensory neurons it functions to sharpen spatial discrimination. Lateral inhibition is influenced by several factors such as the characteristics of cutaneous sensory neurons and stimulation. In order to develop a mathematical model, these are things important to consider. The problem analysis thereby aims to present the neurophysiological background of lateral inhibition. In Section 2.1 the characteristics of cutaneous sensory neurons are described, where the main categories are mechanoreceptors, thermal receptors and nociceptors. They are described with regard to modality, size of their receptive fields, and activation threshold. These are all aspects that vary for the different types of cutaneous sensory neurons and should be considered in process of mathematical modelling lateral inhibition as they may affect the outcome of lateral inhibition. In Section 2.2 the concept of spatial sharpening due to lateral inhibition is elaborated upon along with how two-point stimulation influences spatial acuity. Moreover, the knowledge of spatial summation, distancing between two points and effect dependent on sensory modalities is presented as these mechanisms have all shown to be of interest in the context of lateral inhibition. A better understanding of lateral inhibition and its mechanisms will be investigated, why modelling of lateral inhibition is of interest. The function of lateral inhibition is feed-forward inhibition, which is possible to model in an artificial neural network (ANN). Section 2.3 introduces the development of an ANN model and how as a mathematical modelling tool, ANNs are capable of modelling biological systems. The section covers the basics of ANN, which is the structure of an artificial neuron. Moreover, single-layer and multi-layer ANNs architectures are presented, along with how connectivity impacts the model, and the ability of ANNs to learn by training. Lastly a summary of the problem analysis is presented in Section 2.4. The problem statement derived from the problem analysis is presented in Section 2.5.

2.1 Cutaneous sensory neurons

Cutaneous sensory neurons transduce stimuli presented on the skin into action potentials or graded potentials by their receptors. The skin is the bodies largest sensory organ and several types of cutaneous sensory neurons exist in the skin [Martini et al., 2015]. Each type of cutaneous sensory neuron is structurally different and activated by different modalities and intensities. Common features for cutaneous sensory neurons are their cell body is located in the dorsal root of the spinal cord. Another common feature is that stimuli must occur within the receptive field of cutaneous sensory neurons in order to become activated. The receptive field is defined as an area on the skin, which when stimulated results in excitation of the sensory neuron. [Martini et al., 2015; Feher, 2017] Figure 2.1 illustrates

the receptive fields associated with two cutaneous sensory neurons.

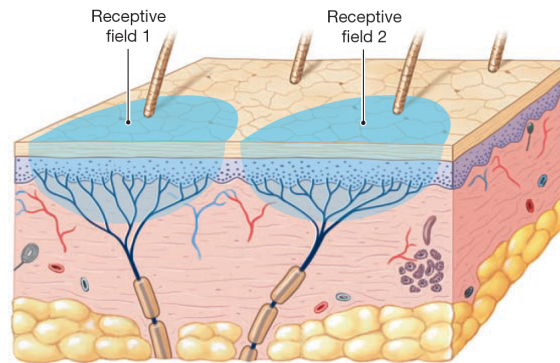


Figure 2.1: Two separate receptive fields. Each of the cutaneous sensory neurons monitor their own individual area. [Martini et al., 2015]

The cutaneous sensory neurons deemed important for the purpose of this thesis are (1) tactile mechanoreceptors, which respond to mechanical stimuli, (2) thermal receptor which respond to temperature related stimuli and (3) nociceptors which respond to any noxious stimuli [Feher, 2017; Kandel et al., 2013].

Mechanoreceptors

Tactile mechanoreceptors are categorized into four primary receptors present in the skin: (1) Meissner corpuscles, (2) Pacinian corpuscles (3) Merkel corpuscles, and (4) Ruffini corpuscles. All of them are unimodal meaning they respond to only one type of stimulus. The characteristics of each primary receptor allows for comprehension of size, shape and textures. The sensory fibers attached to the mechanoreceptors are A- β fibers. [Feher, 2017; Kandel et al., 2013] Figure 2.2 illustrates the structure and location of the primary receptors in both hairy and glabrous skin.

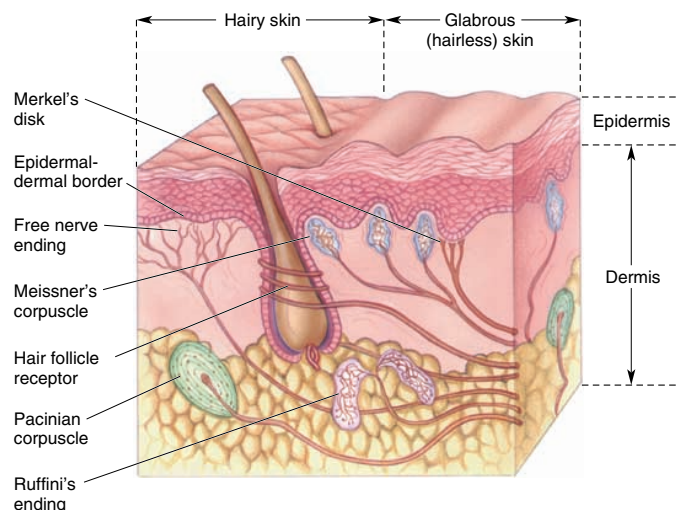


Figure 2.2: The four primary mechanoreceptors and their location in the different layers of both hairy and glabrous skin. [Premkumar, 2004]

Meissner corpuscles and Pacinian corpuscles are present in the subcutaneous layer of the

skin. Meissner corpuscles are primarily located in glabrous skin while Pacinian corpuscles are located in both hairy and glabrous skin [Premkumar, 2004]. They consist of free nerve endings enclosed by a layered capsule. These cutaneous sensory neurons are rapidly adapting and insensitive to static deformation i.e. pressure. However, they are sensitive to dynamic deformation of the skin such as vibratory stimuli. [Feher, 2017] The receptive field of Meissner corpuscles is approximately 3-5 mm in diameter while that of Pacinian corpuscles is larger. The spatial acuity of both Meissner corpuscles and Pacinian corpuscles is low due to the activity of the stimuli being uniformly distributed over the receptive field. [Johnson, 2001]

Merkel corpuscles are located in the dermis and are found in both hairy and glabrous skin [Premkumar, 2004]. These cutaneous sensory neurons are slowly adapting and respond to sustained pressure on the skin. [Feher, 2017] The diameter of the receptive field size of Merkel corpuscles is approximately 2-3 mm. Despite the size of their receptive field the spatial detail of the Merkel corpuscles is approximately 0.5 mm, which results in great spatial acuity, when exposed to pressure related stimuli. [Feher, 2017; Johnson, 2001] Due to having selective sensitivity to strain energy density, which is the energy required to deform the skin locally, the Merkel corpuscles are sensitive to curves, edges and points. Merkel corpuscles have the property of lateral inhibition, which occurs within CNS and enhances contrast and sharpens sensation by suppressing nearby sensory neurons (cf. Section 2.2). [Feher, 2017; Johnson, 2001]

The Ruffini corpuscles are located in the dermis and are found in both hairy and glabrous skin [Premkumar, 2004]. They are slowly adapting and located in the dermis. The diameter of their receptive fields is larger than 10 mm and respond to directional deformations i.e. stretching or tension [Feher, 2017; Johnson, 2001]. They are involved in the perception of touch-pressure related stimuli in collaboration with Merkel corpuscles, though they are more sensitive to horizontal strain than vertical [Johnson, 2001].

Thermal receptors

Thermal receptors are polymodal cutaneous sensory fibers which consist of cold receptors and heat receptors. They allow for comprehension of thermal sensations and overall changes in temperature. Thermal receptors differ from mechanoreceptors by having both slowly adapting as well as rapidly adapting cutaneous sensory neurons. The thermal sensation itself is the combined effects of both types. The rapidly adapting sensory neurons detect an overall change, while the slowly adapting sensory neurons indicate that the stimuli are still present. [Martini et al., 2015; Feher, 2017; Kandel et al., 2013] The sensory fibers responsible for transmission of heat related stimuli are unmyelinated low-threshold C fibers. They are activated at temperatures above 36°C, where the A- δ fibers are activated at temperatures exceeding 45°C. The sensory fiber transmitting innocuous cold-related stimuli are thinly myelinated A- δ fibers. They are activated at temperatures below 36°C. Noxious stimulus is transmitted through unmyelinated high-threshold C-fibers. [Feher, 2017; Kandel et al., 2013]

Nociceptors

Nociceptors are polymodal cutaneous sensory neurons with free nerve endings and have high activation threshold. The fibers responsible for transmissions of noxious stimuli are A- δ and high-threshold C fibers. The A- δ fibers transmit the initial and sharp noxious sensations, while the C fibers have a slower onset but transmit longer lasting sensations. [Feher, 2017; Kandel et al., 2013] The diameter of the receptive field of the nociceptors is approximately 5 mm [Bromm et al., 1984]. The nociceptors are tonic and non-adapting, meaning that the painful sensations will persist until the causing event has ended. [Feher, 2017]

Generally a stimulus at the skin excites cutaneous sensory neurons which results in afferent signals being conveyed to the Thalamus through different sensory pathways. The sensory pathways for noxious and innocuous stimuli along with possible interactions are described in Appendix A. In addition to excitation of cutaneous sensory neurons, inhibitory interneurons are excited and activates lateral inhibition. Lateral inhibition is essential to the perception and localization of stimuli and will be described in the following section. [Feher, 2017; Strominger et al., 2012]

2.2 Lateral inhibition

The concept of neural inhibition is considered as important a neural activity as excitation. The function of the inhibitory interneurons is to modulate the effects of excitation to attain a desired output, which is achieved by preventing the excitatory neurons from excessively firing. Lateral inhibition is a type of neural inhibition and is categorized as feed-forward inhibition. In feed-forward inhibition, one or several neurons inhibit the neural activity of another neuron or several neurons. Feed-forward is expressed in lateral inhibition by the activation of excitatory neurons stimulate the adjacent (lateral) interneurons, which suppress the activity of neighboring neurons. The result is sharpening of spatial discrimination. All sensory systems utilize lateral inhibition in neural processing and in the context of cutaneous sensations lateral inhibition helps localizing stimuli. [Strominger et al., 2012]

On Figure 2.3 a stimulus is applied and the cutaneous sensory neuron whose receptive field center is closest to the stimulus is excited the most. The adjacent cutaneous sensory neurons are excited as well, however the intensities decay symmetrically with distance from stimulus center. Without lateral inhibition the response from the secondary sensory neurons would be proportional to the stimulus intensity from the sensory neurons as in Figure 2.3a. With lateral inhibition the intensity of the stimulus is suppressed by inhibitory interneurons more laterally than at the center sharpening spatial discrimination as illustrated in Figure 2.3c. [Feher, 2017; Strominger et al., 2012] Figure 2.3 furthermore illustrates the spatial distribution of both Figure 2.3a and 2.3c. Without lateral inhibition the spatial distribution of excitation is larger resulting in a decrease in spatial discrimination as shown in Figure 2.3b. A decrease in spatial discrimination reduces spatial acuity. With lateral inhibition the neurons adjacent to the strongly stimulated neuron are inhibited, thereby resulting in a spatial distribution of excitation and inhibition as shown in Figure 2.3d. The spatial distribution of excitation with lateral inhibition is smaller than

without lateral inhibition because of the spatial distribution of inhibition. This enhances the contrast between the strongly stimulated relay neurons and their adjacent weakly stimulated relay neurons, which increases the spatial acuity. [Feher, 2017]

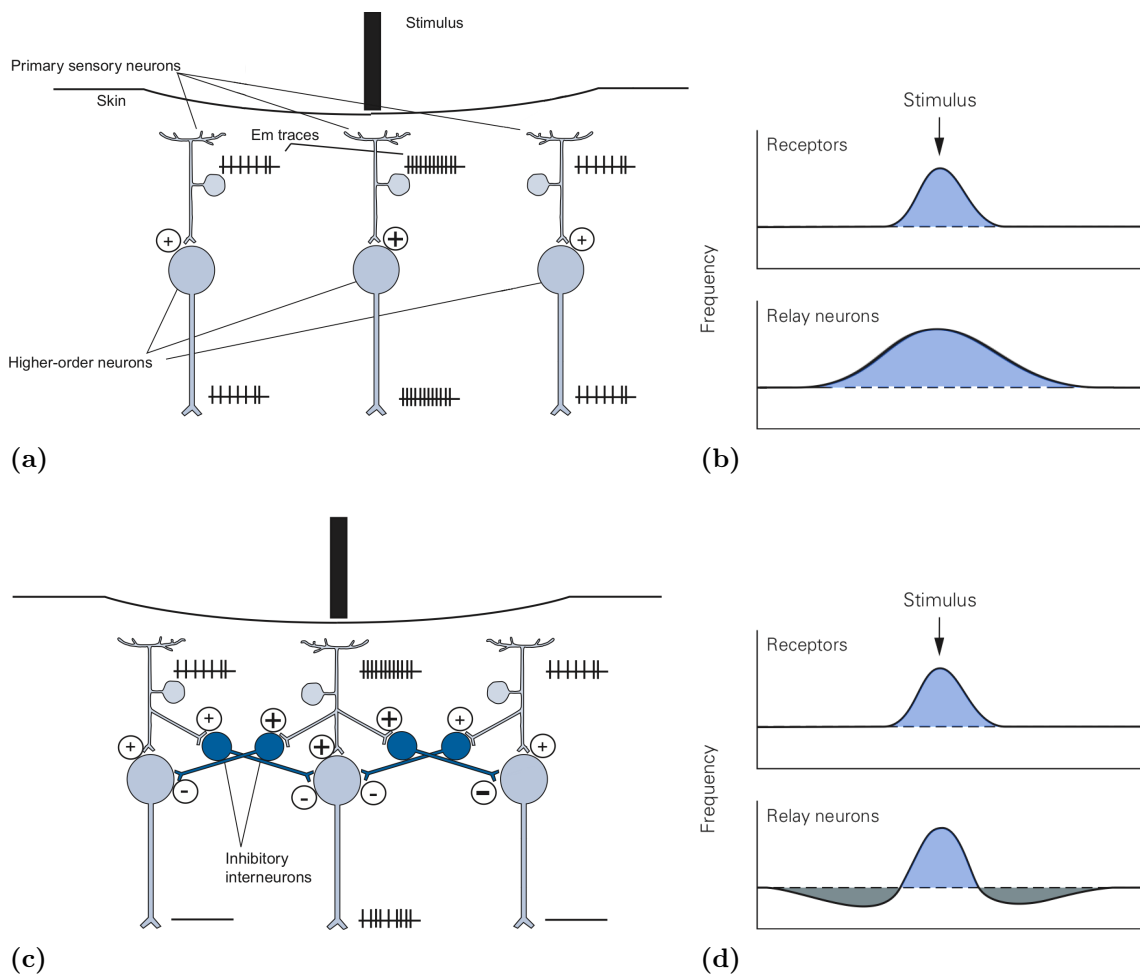


Figure 2.3: (a) Spatial discrimination without lateral inhibition, where the response of the second order neurons would be proportional to the intensity of the stimulus from the sensory neurons resulting in low spatial discrimination. (b) Spatial distribution of excitation without lateral inhibition, where the large distribution from the relay neurons result in a decrease in spatial discrimination. (c) Spatial discrimination with lateral inhibition showing that the inhibitory interneurons inhibit the response of neurons lateral to the stimulus, thus sharpening spatial discrimination. (d) Spatial distribution of excitation and inhibition with lateral inhibition showing that the inhibitory distribution causes the excitatory distribution from the relay neurons to become smaller than without lateral inhibition. This results in an increase in spatial acuity. (a) and (c) modified: Removed text bubbles. [Feher, 2017] (b) and (d) modified: Changed color for excitation from orange to blue. [Kandel et al., 2013]

Acuity of spatial discrimination for single point localization has shown to be greater for innocuous stimuli than that of noxious stimuli. This has been attributed to the somatotopical representation in the brain being lesser for noxious stimuli than innocuous

stimuli. [Koltzenburg et al., 1993]

Spatial acuity is typically evaluated using the two-point discrimination threshold which determines the 50 % threshold of perceiving one two points when the stimulations are simultaneously applied to the skin. [McGee, 2018] The two-point discrimination threshold for noxious and innocuous stimuli has been investigated in several studies [Schlereth et al., 2001; Martikainen and Pertovaara, 2002; Mørch et al., 2010; Mancini et al., 2014]. For simultaneously applied stimuli the threshold for noxious stimuli has shown to be higher than for innocuous stimuli [Schlereth et al., 2001; Mancini et al., 2014; Frahm et al., 2017], when comparing to studies where sequential stimuli was applied [Martikainen and Pertovaara, 2002; Mørch et al., 2010]. This implies that a temporal component may affect the two-point discrimination threshold for noxious and innocuous stimuli.

In the study by Frahm et al. [2017] the spatial acuity of innocuous stimuli and noxious stimuli, was investigated, where the distance between the two points was incremented from 10-100 mm. It is indicated that the spatial acuity might be affected by the mechanisms of lateral inhibition and spatial summation. [Frahm et al., 2017; Quevedo et al., 2017]

Spatial summation of sensory information is characterized as perception of increased intensity, when the stimulation size of the stimulated area is expanded. There are two general neural mechanisms which account for spatial summation of sensory information (1) local integration and (2) neuron recruitment which area illustrated on Figure 2.4.

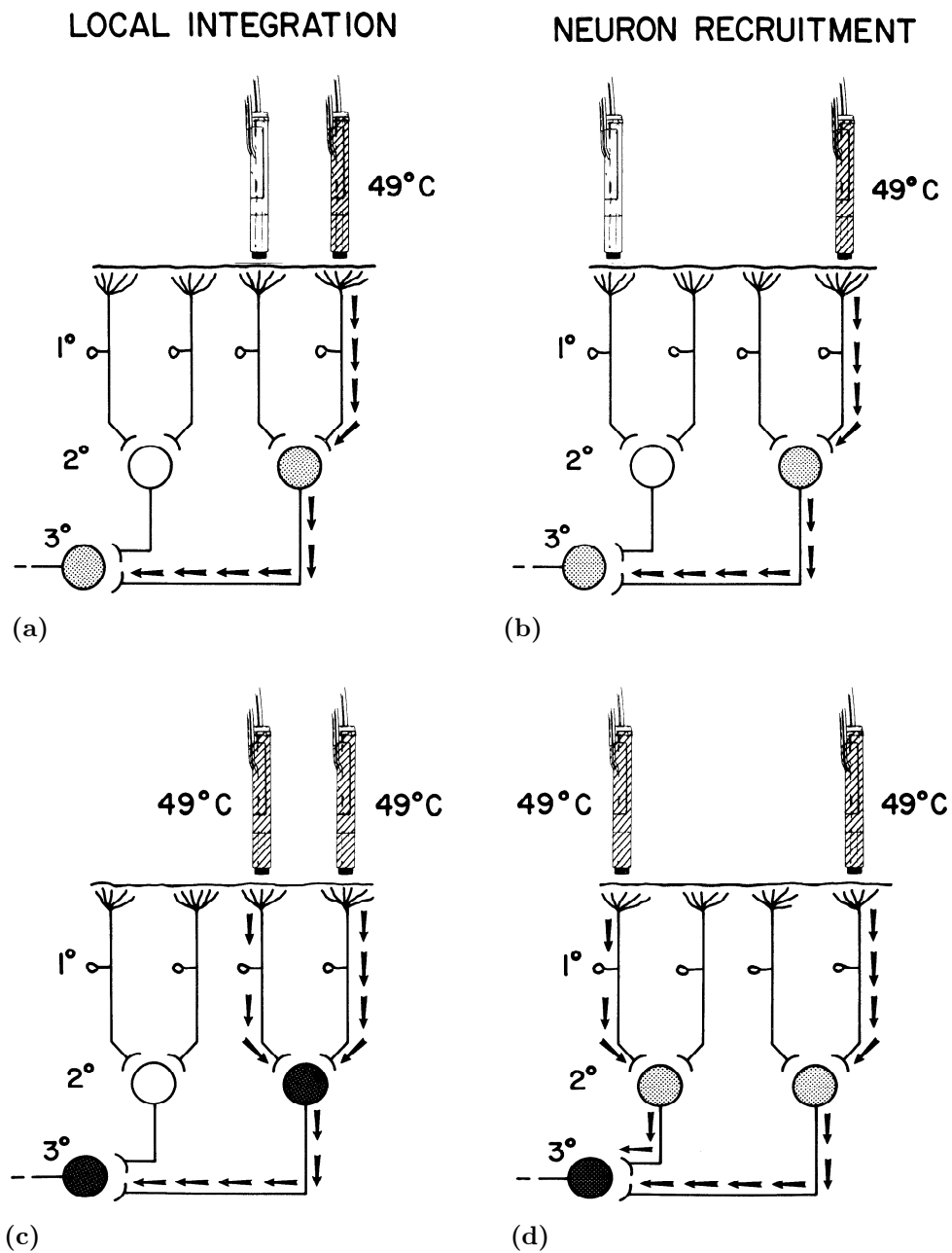


Figure 2.4: Schematic representation spatial summation with local integration and neuronal recruitment. (a) illustrates local integration a single stimulation is applied on a small area of the receptive field leads to a small degree of spatial summation. (c) illustrates stimulation applied on a larger area of the of the receptive field causes a large summation. Thereby the degree of spatial summation from local integration is limited by the area of the receptive field. (b) shows neuron recruitment where a single stimulation is applied. In neuron recruitment the degree of spatial summation is related to the entire area stimulated. A small area results in small spatial summation, while a larger area will result in high spatial summation. On (d) two stimulations are applied, where the entire stimulation area now has become larger. This results in higher neuron recruitment and greater degree of spatial summation. [Price et al., 1989]

Figure 2.4a illustrates the effect of local integration for a single stimulation on a small area of a receptive field. The summation is small, which is indicated by the grey node. Figure 2.4c illustrates local integration where second receptive field is stimulated. In local integration the individual sensory neurons integrate afferent input from stimulus areas within their receptive field. This means that the spatial summation is limited by the size of the area of the receptive field, that is stimulated for each individual neuron. Thereby the summation in Figure 2.4a is lower than in Figure 2.4c which is indicated by the activation of the second order neuron (black node). Neuron recruitment is another mechanism where the spatial summation depends on the entire area stimulated. Increasing the total stimulation area leads to an increased number of activated neurons. In Figure 2.4b only a single stimulation is applied and the total area of stimulation is small leading to small summation, which is indicated by the single grey node. In Figure 2.4d two simultaneously applied stimulation over a distance result in an increased overall stimulation area. This results in high amount of spatial summation. [Price et al., 1989]

The existence of spatial summation has been well established for innocuous stimuli. With regard to noxious stimuli, previous studies concluded that spatial summation was non-existent [Hardy et al., 1940] Recent studies indicate that the spatial summation for noxious stimuli does indeed exist, however the degree of spatial summation is influenced by different characteristics such as distancing and spatial pattern of the stimuli. [Quevedo et al., 2017]. An example of this for noxious and innocuous stimuli may be two stimuli activating receptive fields, which are overlapping. The overlap in receptive fields result in overlapping excitatory and inhibitory fields as illustrated in Figure 2.5. The activity in the overlapping excitatory and inhibitory fields will be summated through the process of spatial summation, which may explain a decrease in spatial acuity. [Martini et al., 2015; Feher, 2017; Frahm et al., 2017] This may be related to the concept of neuron recruitment, where the total number of activated neurons are dependent on the size of the stimulated area.

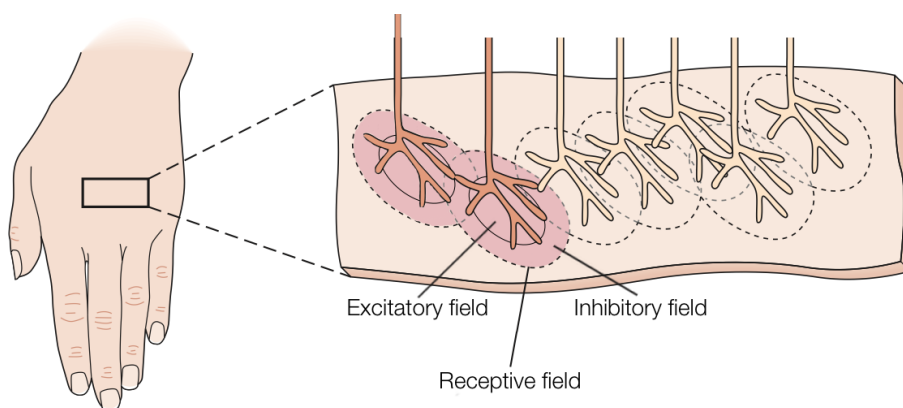


Figure 2.5: Overlapping excitatory and inhibitory fields resulting in decreased spatial acuity due to spatial summation between overlapping fields. Modified: Added a stimulated receptive field as well as excitatory and inhibitory fields. [Kandel et al., 2013]

Spatial summation for two-point noxious heat stimuli is progressively larger at separation distances from 10 mm to 100 mm, and subadditive for distances greater than 100 mm

which may be explained by a change in number of recruited neurons [Quevedo et al., 2017]. Spatial summation for two-point tactile stimulation has shown to be present at separation distances of 60 mm to 120 mm, however the summation does not vary significantly across separation distance [Mørch et al., 2010].

This implies that spatial summation for noxious and innocuous stimuli is different, which may be related to the two types of stimuli being conducted through different sensory pathways. Lateral inhibition is present in both of these sensory pathways, however it is uncertain how its impact on spatial discrimination is different between noxious and innocuous stimuli. By modelling lateral inhibition in the spinal cord for both noxious and innocuous stimuli it may be possible to gain insight on the impact of lateral inhibition for both sensory pathways. Since lateral inhibition is categorized as feed-forward inhibition, it is possible to model it as an artificial neural network (ANN). The following section describes how ANNs are used as a mathematical modelling tool as well as their capability to model biological systems.

2.3 Artificial neural network model development

An artificial neural network (ANN) can be defined as models based on the human nervous system [Negnevitsky, 2005]. The basic premise of ANNs is to provide an input and have the network transforming it to a desired output. ANNs can be applied to various areas such as (1) classification (2) curvefitting and (3) prediction systems. [da Silva et al., 2017] The structure of an artificial neuron is nonlinear and gathers information available on its input and produce an output based on its activation function. The simplest ANN was created by Rosenblatt [1958] and known as the perceptron or the artificial neuron. The structure of an artificial neuron is illustrated in Figure 2.6. [da Silva et al., 2017]

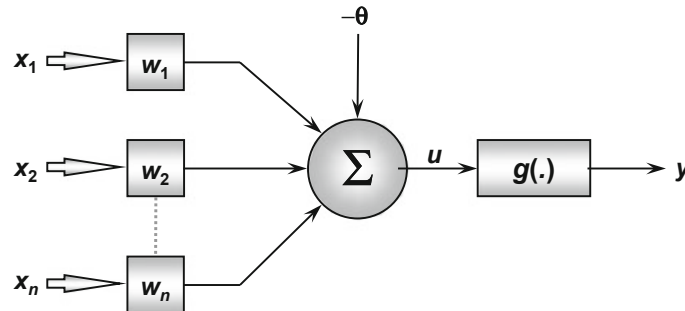


Figure 2.6: Model of an artificial neuron. The model is comprised of x_n input each with w_n weight summated in the output neuron, where its output is limited by an activation function $g()$ giving the final output y . [da Silva et al., 2017]

As shown in Figure 2.6 an artificial neuron receives external inputs signal (x_1, x_2, \dots, x_n) . The values of the synaptic weights are then used to weigh each of the inputs thereby emphasizing certain inputs. The linear aggregator Σ summates all the weighted inputs and calculates an activation, which based on the activation threshold θ generates a value to the output neuron if the activation exceeds the threshold. The activation potential u is the difference between the linear aggregator and the activation threshold. If $u \geq 0$ the neuron produces a positive output otherwise the output will be negative. u being a weighted sum

of its inputs as the output of the neuron, is also the input to the activation function $g()$. The activation function creates non-linearities by limiting the output of the neuron within a range of values. The output of $g()$ is, y , the final output produced by the neuron. The output of one neuron may function as input in a successive neuron. [da Silva et al., 2017]

McCulloch and Pitts [1943] expressed the activation function as in equation (2.1) and the output as in equation (2.2):

$$u = \sum_{i=1}^n w_i \cdot x_i - \theta \quad (2.1)$$

$$y = g(u) \quad (2.2)$$

Activation function

The output of every neuron passes through an activation function before further proceeding as an input in a model. Activation functions are categorized as either partially or fully differentiable. An activation function is characterized as partially differentiable if the function does not have first order derivatives in their domain. On the contrary, activation functions that have existing first order derivatives for all points in their domain, are defined as fully differentiable. The use of activation functions depends on the learning algorithm used for training the ANN. [da Silva et al., 2017]

The symmetric ramp function is a commonly used partially differentiable activation function. The activation function returns the activation potential as the output value, when between a defined range $[-a, a]$. The output is also limited by the range. [da Silva et al., 2017] The mathematical expression of a symmetric ramp function is therefore given as [da Silva et al., 2017]:

$$g(u) = \begin{cases} a, & \text{if } u > a \\ u, & \text{if } -a \leq u \leq a \\ -a, & \text{if } u < -a \end{cases} \quad (2.3)$$

The symmetric ramp function is illustrated in Figure 2.7 with the defined range $[-a, a]$.

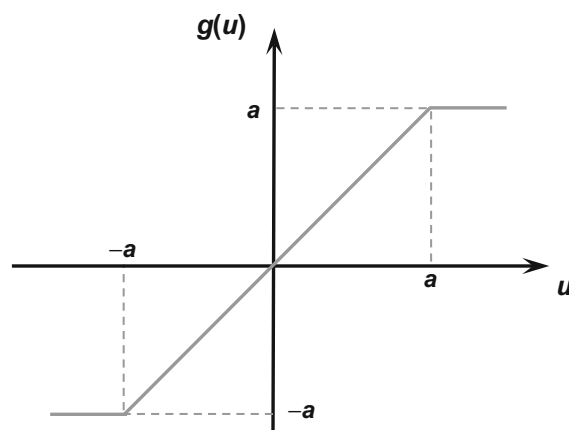


Figure 2.7: Symmetric ramp function limiting $g(u)$ to be between $-a$ and a . [da Silva et al., 2017]

The common fully differentiable activation function is the logistic or hyperbolic tangent function, both derived from the family of functions termed sigmoidal. The logistic function has real values between 0 and 1 as output. The slope of the function in its inflection point can be altered by a real constant β . [da Silva et al., 2017] The mathematical expression of a logistic function is therefore given as [da Silva et al., 2017]:

$$g(u) = \frac{1}{1 + e^{-\beta \cdot u}} \quad (2.4)$$

The logistic function is illustrated in Figure 2.8a with β and the inflection point. Figure 2.8b shows how an increase of β affects the slope of the logistic function. It is theoretically possible to obtain a likewise function as the symmetric ramp function by having a very high value for β that is going towards infinity. The difference would be that the logistic function is fully differentiable in its entire domain compared to the symmetric ramp function, which is partially differentiable. [da Silva et al., 2017]

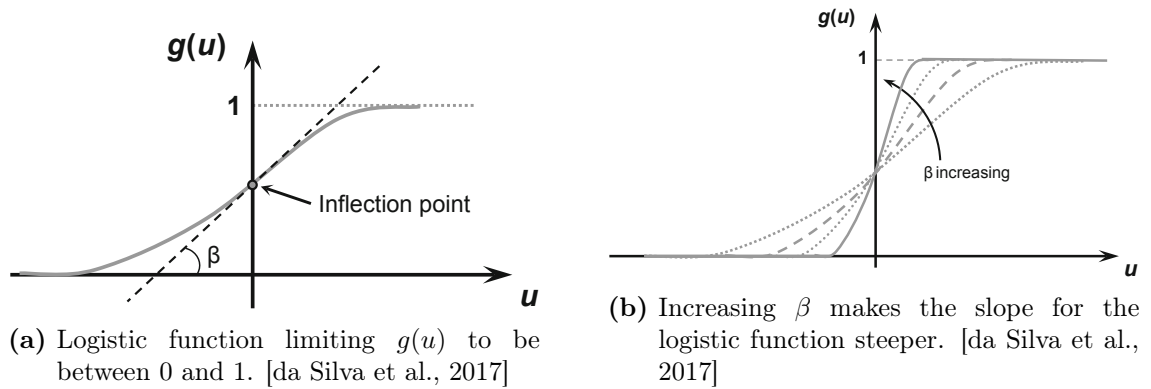


Figure 2.8

The hyperbolic tangent function has real values between -1 and 1 as output, where the slope similar to logistic function can be altered by a real constant β . [da Silva et al., 2017] The mathematical expression of a hyperbolic tangent function is equation 2.4 just scaled and shifted given as [da Silva et al., 2017]:

$$g(u) = \frac{1 - e^{-\beta \cdot u}}{1 + e^{-\beta \cdot u}} \quad (2.5)$$

The hyperbolic tangent function is illustrated in Figure 2.9a with β and the inflection point. Figure 2.9b shows how an increase of β affects the slope of the hyperbolic tangent function.

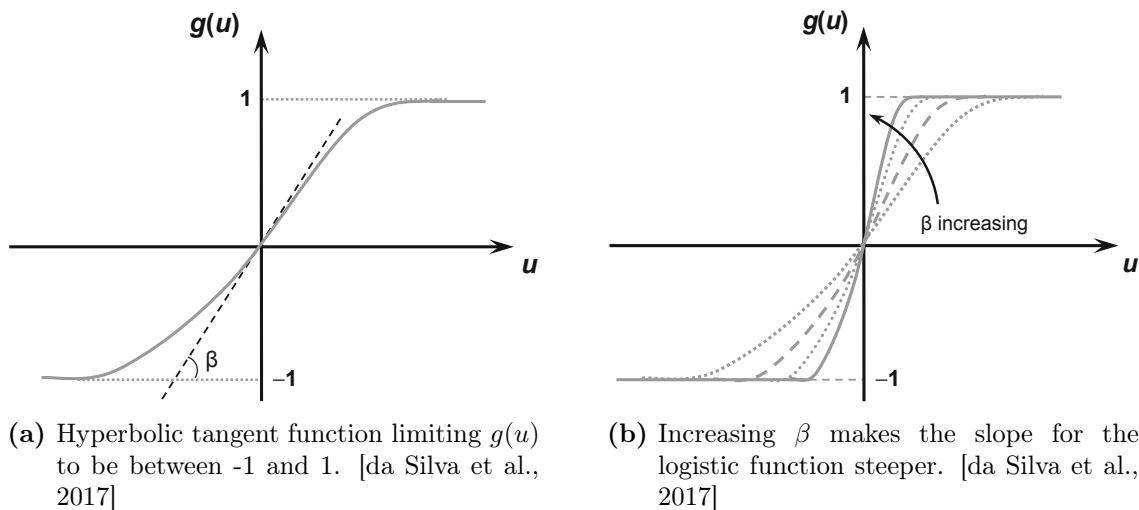


Figure 2.9

Architectures of artificial neural network

The arrangement of artificial neurons in relation to each other is defined by the architecture of the ANN. A neural network consists of several layers with several artificial neurons within the layer, all which are interconnected. A simple architecture of an ANN is a single-layer ANN, which consists of two layers; an input and output layer with weighted connections between them. Computation is done by the output layer and not in the input layer, why it is called a single-layer ANN [Sazli, 2006]. A single-layer ANN is illustrated in Figure 2.10 with a feedforward architecture. A feedforward ANN allows signals to flow in a single direction being from input to output. In addition, there is no feedback loop, which prevents the output of a layer to affect the layer it originated from. The input layer receives external information such as signals or measurements and passes them on to the next layer, which is the output layer. The input of the input layer is typically normalized for the purpose of better numerical precision for the mathematical operations performed by the network. The output layer produces the output by applying the weighted sum of the input to an activation function. [da Silva et al., 2017; Negnevitsky, 2005; Sazli, 2006]

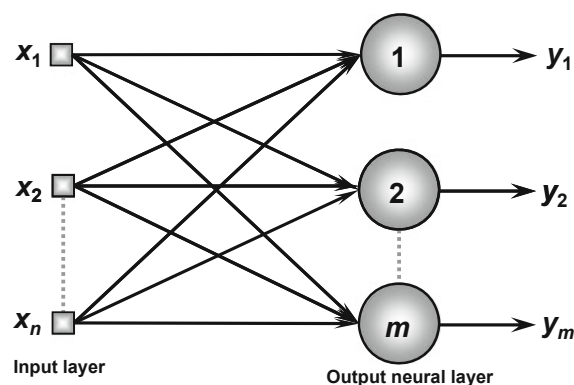


Figure 2.10: A fully connected single-layer feedforward ANN with n inputs and m outputs. [da Silva et al., 2017]

Another general architecture of an ANN is the multi-layer ANN. The multi-layer ANN

differentiates from the single-layer ANN by consisting of one or more hidden layers with hidden neurons between the input and output layer. The input layer serves the same purpose as in the single-layer ANN and feeds into one or more hidden layers. The hidden layers are responsible for performing most of the internal processing from the network. By having a single hidden layer, it is possible to represent the inputs as a function. The final layer is the output layer, which produces an output based on the processing performed by the previous layers. [da Silva et al., 2017; Negnevitsky, 2005] A multi-layer feedforward ANN with two single hidden layers is illustrated in Figure 2.11.

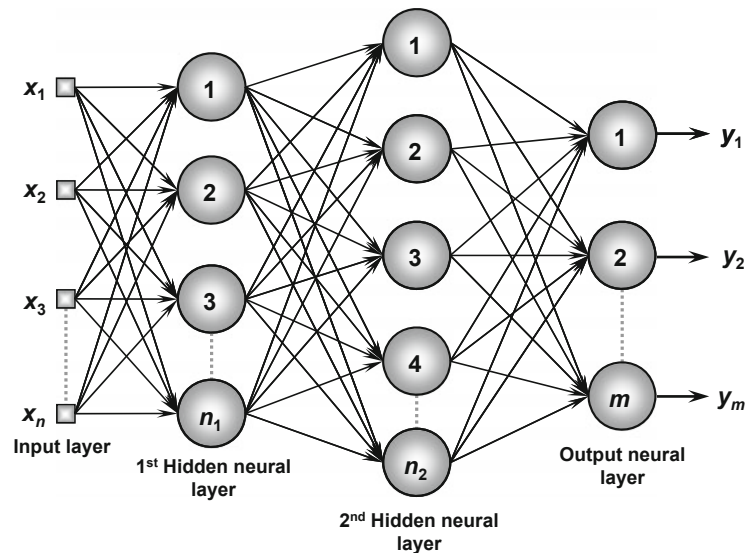


Figure 2.11: A fully connected multi-layer feedforward ANN with two hidden layers. The ANN is composed of n inputs, n_1 hidden neurons in the first hidden layer, n_2 hidden neurons in the second hidden layer and m outputs. [da Silva et al., 2017]

A fully connected ANN is when each neuron is connected to every neuron in the next layer as shown in Figure 2.10 and 2.11. It is important to note that ANNs do not have to be fully connected. It is possible to have no connections between a neuron and another neuron in the next layer, establishing a partially connected ANN. [Sazli, 2006] A fully connected ANN may introduce high redundancy and complexity. If this is not desired in the ANN model, then a partially connected ANN can be implemented with the aim of reducing the ANN topology and number of connections, while obtaining the same performance or better than the fully connected ANN. Reducing the number of connections may lower the complexity of ANNs, enhance generalization, decrease training time, and result in a model approaching biological reality. [Elizondo and Fiesler, 1997]

2.4 Summary

Cutaneous sensory neurons transduce stimuli perceived on the skin into action potentials or graded potentials by their receptors. The receptors of relevance for this thesis are tactile mechanoreceptors, thermal receptors, and nociceptors. These respond to mechanical stimuli, temperature related stimuli and any noxious stimuli respectively. Properties common for all three receptors are the location of the cell body in the dorsal root of

the spinal cord. Furthermore, each type of receptor have a receptive field, which differs in size and shape between receptors. The receptive field itself is an area on the skin that excites the sensory neuron when stimulated. During stimulation of a receptive field a surrounding inhibitory field is activated, which activates lateral inhibition that sharpens spatial discrimination and increases spatial acuity. The activation of lateral inhibition excites excitatory neurons, which stimulate the adjacent interneurons and suppressing the activity of neighboring neurons. Spatial discrimination can be evaluated with the two-point discrimination threshold, which determines the 50 % threshold of perceiving one two points when the stimulations are simultaneously applied to the skin. Spatial acuity might be affected by lateral inhibition due to spatial summation of overlapping excitatory and inhibitory fields. Lateral inhibition is expressed as a biological feed-forward inhibition system, which can be mathematically modelled with artificial neural networks (ANNs). An ANN is a mathematical model based on the human nervous system and consists of artificial neurons, which can be structured as a single-layer or multi-layer ANN. ANNs are capable of learning and thereby establishing a relationship, and possibly explain the difference between input and output. Due to its similarities to the human nervous system it is feasible to use in modelling of lateral inhibition.

Lateral inhibition is present in the sensory pathways of both noxious and innocuous stimuli, however it is uncertain how its impact on spatial discrimination differs. By modelling lateral inhibition in the spinal cord for both noxious and innocuous stimuli using ANN it may be possible to gain insight on how lateral inhibition impacts spatial discrimination for both sensory pathways. This leads to the following problem statement.

2.5 Problem statement

How can artificial neural network models be implemented to investigate the effect of lateral inhibition on the discriminatory differences between noxious and innocuous stimuli?

Methodology 3

In this chapter a model of lateral inhibition is developed by implementation of an artificial neural network (ANN) in order to investigate the discriminatory differences between noxious and innocuous stimuli. The investigation of discriminatory differences between noxious laser stimulation and innocuous mechanical pressure stimulation was conducted by means of two-point discrimination data, which was used for training and validating the model. The specifics of the training data and the means by which it was acquired is explained in Section 3.1. A brief overview of the lateral inhibition model development process is presented in Section 3.2 and the design and development of the lateral inhibition model is elaborated in Section 3.3. The input layer models the sensory input on the skin. Laser stimulation and mechanical stimulation activate nociceptors and tactile mechanoreceptors respectively that both have different characteristics that must be taken into consideration. For the lateral inhibition model the receptive field diameter innervated by the different modalities are considered of importance for the input layer. The output layer models lateral inhibition using the Mexican-hat model introduced by Kohonen [1982] whose output describes lateral inhibition with a Mexican-hat function. Moreover the implementation of the model is explained. After implementing the model it was trained using the Gradient descent method as learning algorithm which is elaborated upon in Section 3.4. The model output must be analyzed after training to determine how well the model was trained. The specifics of the data analysis is elaborated upon in Section 3.5. Moreover a sensitivity analysis is performed to determine how sensitive the model output is to changes in the input. The specifics of the sensitivity analysis is elaborated upon in Section 3.6. The model must be validated to evaluate its performance, where the model validation is achieved using two-point discrimination data found in literature as explained in Section 3.7.

3.1 Data acquisition

Two-point discrimination data was acquired from the study by Frahm et al. [2017]. The data was collected at Department of Health Science and Technology, Center for Neuroplasticity and Pain (CNAP), SMI, Integrative Neuroscience Group at Aalborg University, Aalborg, Denmark. The data was from 13 healthy subjects and collected using painful heat and nonpainful mechanical touch stimulation on the right volar forearm. The two-point discrimination threshold for noxious heat stimulation was tested using a Synrad Firestar ti-series 100 W CO₂ laser with a beam diameter of 5 mm. The two-point discrimination threshold for mechanical touch in Frahm et al. [2017] was tested using a Vernier caliper with 2 blunt plastic filaments with a diameter of 5 mm. A point-to-point distance between 10 and 100 mm, in steps of 10 mm was used. The two-point discrimination

data was fitted to a sigmoidal curve, which is presented in Figure 3.1a for laser stimulation and Figure 3.1b for mechanical stimulation. The details of the experiment is elaborated upon in Appendix B.

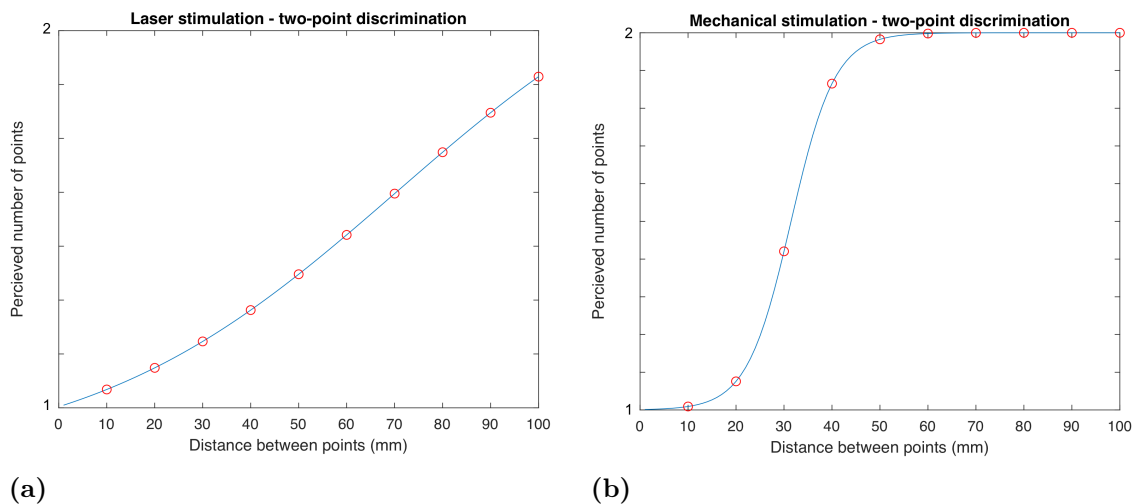


Figure 3.1: (a) Two-point discrimination data for noxious laser stimulation and (b) two-point discrimination data for mechanical stimulation from Frahm et al. [2017].

3.2 Model overview

Lateral inhibition was modelled as a single-layer ANN. The neurons in the input layer models the receptive fields for both tactile mechanoreceptors and nociceptors. The output layer models the spatial distribution of excitation for two simultaneously applied stimulations and probability of perceiving one or two points. The lateral inhibition model is trained with two-point discrimination data and thereafter validated to verify its capability of discriminating differences between noxious and innocuous stimuli. The lateral inhibition model was developed and trained in MATLAB R2017b (MathWorks inc.). The overview of the model development is illustrated in Figure 3.2.

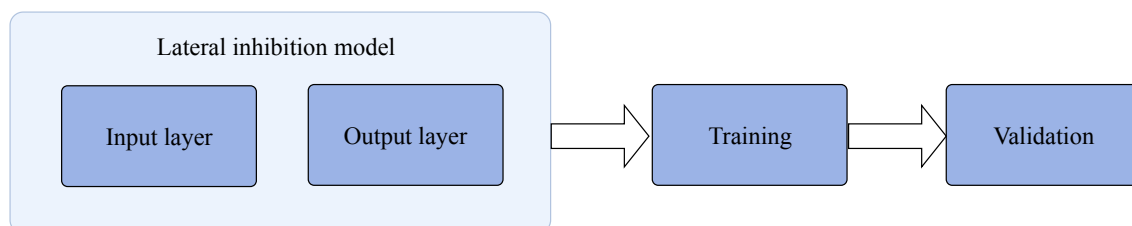


Figure 3.2: Overview of the model development process.

3.3 Lateral inhibition model

In the following, the model design of the input and output layer are explained. The input layer models the receptive fields of both nociceptors and tactile mechanoreceptors. Thereby the diameter of the neurons in the input layer are diameter of the receptive field of either tactile mechanoreceptors or nociceptors which chosen to be 2.5 mm and 5 mm

respectively. It is well known that receptive fields overlap [Kandel et al., 2013], however no overlap is assumed in the model. The diameter of both laser stimulation and mechanical stimulation was 5 mm, which may cause more than a single neuron to be activated when per stimulation. An example is illustrated in Figure 3.3, for at receptive field of tactile mechanoreceptors with a diameter of are 2.5 mm resulting in the activation of either two or three neurons depending on the stimulation position. The same applies for nociceptors, however since their receptive field diameter is 5 mm either one or two neurons will become activated depending on the position of the stimulation. No stimulation shift is assumed in model.

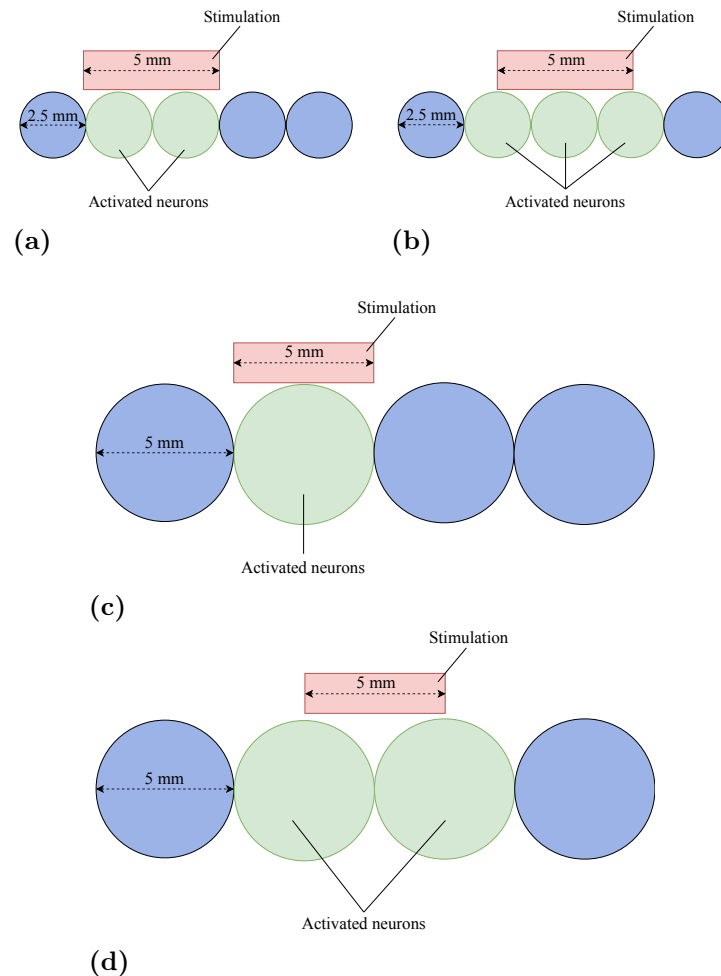


Figure 3.3: (a) Stimulation diameter of 5 mm activates two receptive fields of mechanoreceptors each with a diameter of 2.5 mm causing activation of two neurons. (b) By shifting the stimulation position a maximum of three neurons become activated. (c) Stimulation diameter of 5 mm activates the receptive field of a single nociceptor, thereby activating a single neuron. (d) By shifting the stimulation position a maximum of two neurons become activated.

The output layer is modelled as a Mexican-hat model, which results in a spatial distribution of excitation with a lateral inhibition effect similar to that presented in Figure 2.3d.

Input layer

The input layer receives either two laser stimulation or two mechanical pressure stimulation (henceforth mechanical stimulation). Applying mechanical stimulation to the skin causes deformation over a skin area, which lead to excitation of cutaneous sensory neurons [Feher, 2017]. The laser stimulations were applied with a Gaussian-like profile and likewise excited cutaneous sensory neurons [Frahm et al., 2017]. The intensity of the stimulations decay symmetrically from the center of both laser and mechanical stimulation [Feher, 2017]. Thereby the stimulations applied to in model input will have a symmetrical decay from the stimulus center. The input layer models the receptive fields of the skin and mimics symmetrical decay by specific synaptic weights. The neurons in the input layer models the receptive fields of cutaneous sensory neurons, where i number of neurons depends on the modality. This is due to the the receptive field diameter of nociceptors and tactile mechanoreceptors being different (cf. Section 2.1).

In order to obtain a symmetrical decay from a stimulus center there must be at least three synaptic weights, $w_j \geq 3$. An example of an input layer with x_i neurons and three symmetrically synaptic weights is illustrated in Figure 3.4, where w_1 , w_2 and w_3 represents the symmetrical decay around the stimulus center, why $w_1 > w_2 > w_3$ applies. The input layer is connected directly to the output layer with the weighted connections hence a single-layer ANN.

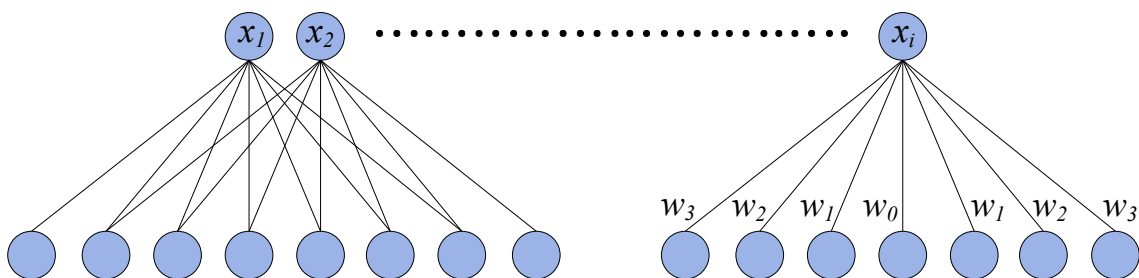


Figure 3.4: Input layer with x_i neurons and three synaptic weights with w_1 , w_2 and w_3 as weights. The number of weighted connections in the input layer depends on the model design. The input layer is connected to the output layer, thereby it is a single-layer ANN.

Output layer

The output layer is modelled as the Mexican-hat model from the Kohonen network introduced by Kohonen [1982] and elaborated upon in Appendix C. The Mexican-hat model is applicable because of its excitatory and inhibitory lateral connections between the output neurons. Figure 3.5 illustrates the Mexican-hat model and its lateral connections, where s_i is the input corresponding to output from the previous layer, and x_i is the stimulus center. The lateral connections to the stimulus center produce an excitatory and inhibitory effect on adjacent neurons depending on proximity similar to the lateral inhibition mechanism. The excitatory effect is applied at the neuron corresponding to the stimulus center and a defined region of neurons in close proximity as illustrated in Figure 3.5a. The inhibitory effect is applied on both lateral sides further away from the stimulus center by a defined region as shown in Figure 3.5b. The inhibitory region range from x_i to x_{i-k} and x_{i+k}

for $k = 1, \dots, R_2$, where R_2 is the radius. The excitatory region is defined as $R_1 < R_2$. The synaptic weights w_k are positive for $0 \leq k \leq R_1$, and negative for $R_1 < k \leq R_2$. The Mexican-hat model combines both excitatory and inhibitory regions and illustrated in Figure 3.5c. [Fausett, 1994]

The synaptic weights between neurons in the Mexican-hat model can be described by the Mexican-hat function as depicted under the Mexican-hat model in Figure 3.5. The Mexican-hat function of lateral inhibition is illustrated in Figure 3.5c as a summation of the excitatory region and inhibitory region resulting in an excitatory region around the stimulus center and an inhibitory region outside of the excitatory region. [Fausett, 1994]

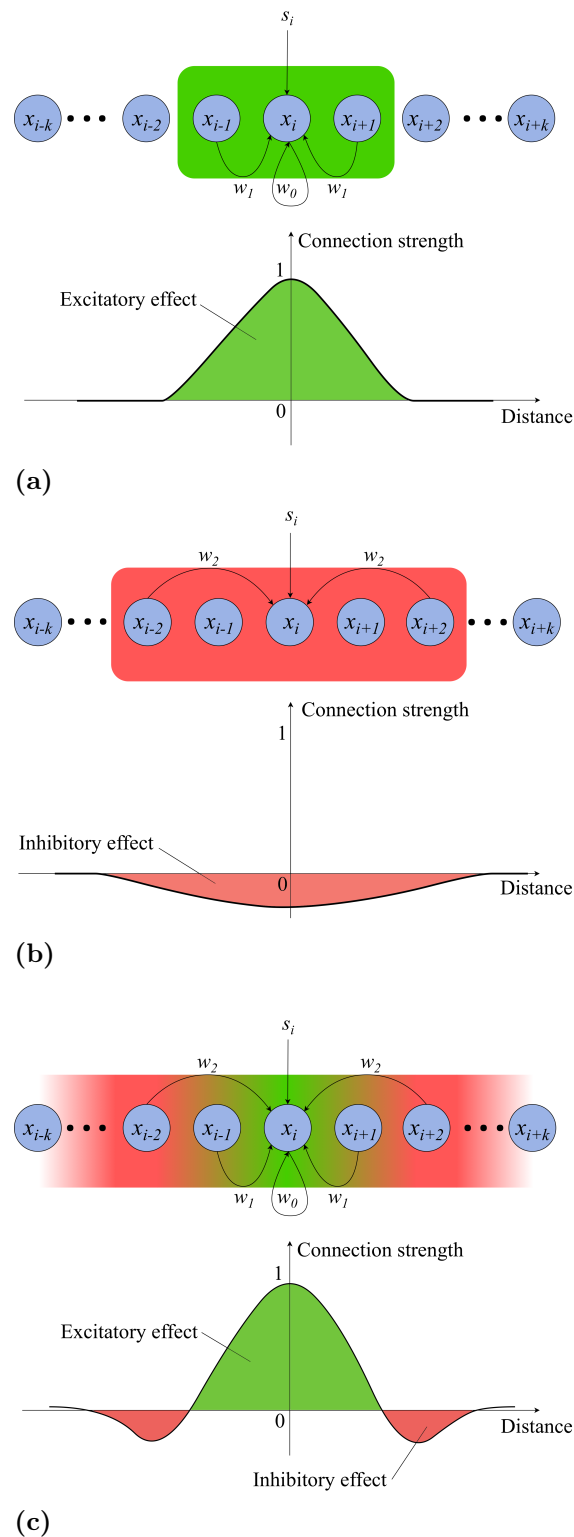


Figure 3.5: Mexican-hat model, where s_i is the input and x_i is the stimulus center, radius of excitatory region $R_1 = 1$, radius of inhibitory region $R_2 = 2$. (a) The lateral connections with the synaptic weights w_1 connected to the stimulus center produce an excitatory effect on adjacent neurons. (b) The lateral connections with the synaptic weights w_2 connected to the stimulus center produce an inhibitory effect on adjacent neurons. (c) The Mexican-hat model combining both excitatory and inhibitory regions resulting in the Mexican-hat function as output. Adapted from Fausett [1994].

The activation of neuron x_i at an iteration t iterated several times is expressed by [Fausett, 1994]:

$$x_i(t) = f[s_i(t) + \sum_k w_k \cdot x_{i+k}(t-1)] \quad (3.1)$$

where the terms in the summation calculates the net input, which are the weighted sum of the neurons x_{i+k} for $k = -R_2, \dots, R_2$ at the previous iteration. A number of iterations are used to achieve an enhanced contrast. [Fausett, 1994] Modeling lateral inhibition does not require contrast enhancement since the model is a feed-forward network and is therefore only iterated once. Therefore equation (3.1) can be expressed as:

$$x_i = f[s_i + \sum_k w_k \cdot x_{i+k}] \quad (3.2)$$

A symmetrical Mexican-hat function as the output by the Mexican-hat model may be achieved by defining one fixed weight for all synaptic weights in the excitatory region and another fixed weight for all synaptic weights in the inhibitory region. Defining w_1 for the excitatory region and w_2 for the inhibitory region the net input in equation (3.1) for $i = 1, \dots, n$ can be expressed as [Fausett, 1994]:

$$x_i = w_1 \sum_{k=-R_1}^{R_1} x_{i+k} + w_2 \sum_{k=-R_2}^{-R_1-1} x_{i+k} + w_2 \sum_{k=R_1+1}^{R_2} x_{i+k} \quad (3.3)$$

The activation potential of the neuron x_i is obtained by an activation function $f(x)$. Since the minimum and maximum activation potential of a neuron is defined as 0 and 1, it is evident to use a ramp function with a range of $[0, 1]$. The mathematical expression of a ramp function is given as [Fausett, 1994]:

$$g(u) = \begin{cases} a, & \text{if } u > a \\ u, & \text{if } 0 \leq u \leq a \\ 0, & \text{if } u < 0 \end{cases} \quad (3.4)$$

The ramp function is illustrated in Figure 3.6 with a defined range between $[0, a]$.

where i was multiplied by an arbitrary number 3 in order to ensure that there was enough neurons to cover the R_2 region. Therefore it was possible to achieve an equal number of neurons in the input and output layer. To simplify the model, the input layer was implemented so that stimulations as impacted the model with no symmetrical decay from stimulus center, which means that $w_1 = w_2 = w_3 = 0$. The initial parameters used to implement the input layer are defined in Table 3.1.

Table 3.1: Parameters used in the initial implementation of the input layer.

| Parameter | Laser stimulation | Mechanical stimulation | Description |
|-----------|-------------------|------------------------|---|
| D | 5 mm | 2.5 mm | Receptive field diameter. |
| i | 60 | 120 | Total number of neurons. |
| w_1 | 0 | 0 | Synaptic weight ($w_1 > w_2$ for $w_1, w_2 \neq 0$). |
| w_2 | 0 | 0 | Synaptic weight ($w_1 > w_2 > w_3$ for $w_1, w_2, w_3 \neq 0$). |
| w_3 | 0 | 0 | Synaptic weight ($w_3 < w_2$ for $w_3, w_2 \neq 0$). |

The output layer receives the weighted sum from the input layer, where the stimulus center of each stimulation correspond to x_i in the Mexican-hat model obtaining excitatory and inhibitory effect on neurons adjacent to the stimulus center depending on proximity. The Mexican-hat model was implemented based on the pseudocode presented in Algorithm 1 but differed slightly by using equation (3.1) instead of equation (3.3), resulting in $2 \cdot R_1 + 1$ number of excitatory weights and $2 \cdot R_2 + 1$ number of inhibitory weights, instead of two fixed weights. The excitatory weights were randomly generated numbers in the range of $[0, 1]$ and sorted to achieve symmetrical decay from the stimulus center. The inhibitory weights were randomly generated numbers in the range of $[-\text{minimum generated excitatory weight}, 0]$ and sorted to be symmetrically rising from the stimulus center. The ranges ensured that the excitatory and inhibitory weights when applied and summed does not cancel each other out.

An overview of the initial parameters used to implement the output layer are defined in Table 3.2.

Table 3.2: Parameters used in the implementation of the output layer.

| Parameter | Laser stimulation | Mechanical stimulation | Description |
|-----------|-------------------|------------------------|--|
| i | 60 | 120 | Total number of neurons. |
| R_1 | 1 | 1 | Radius of the excitatory region |
| R_2 | 5 | 5 | Radius of the inhibitory region |
| x_{max} | 1 | 1 | Upper limit of the activation function |

3.4 Model training

Some of the key features of an ANN is its ability to learn from the inputs it receives and establish a relationship between input and output. By training an ANN it becomes capable of generalizing solutions. Thereby the ANN is able to produce an approximation of a desired output from the input it is given. The process of training an ANN uses learning algorithms to train the model, which is done by tuning the synaptic weights. Generally the aim is to obtain the synaptic weights, which provides the best generalized solutions. [da Silva et al., 2017] In relation to the lateral inhibition model the aim is to obtain a set of excitatory and inhibitory weights in the output layer which can provide the best generalized solutions for all point-to-point distances for a given stimulus modality.

A set of all available data reflecting the behavior of a system is separated into two groups; training data and test data. The training data is utilized during the learning process of an ANN. The ability of an ANN to generalize solutions within acceptable degrees is verified with the test data and provides a validation of the ANN topology. [da Silva et al., 2017]

Training data

The data used for training is the probability of perceiving one or two points. Training data for both noxious and innocuous stimuli is based on a fitted sigmoidal curve used to analyze the responses to the two-point discrimination. The training data was acquired from the study by Frahm et al. [2017] (cf. Section 3.1). The equation for the sigmoidal curve is given by:

$$t = \frac{1}{1 + e^{(a(b-x))}} \quad (3.6)$$

where t is the probability of perceiving one or two-points, and b correspond to $t = 0.5$ which is the 50 % threshold of the subjects perceiving one or two points. At $t = 1$ the probability of perceiving two points is 100 %. The slope of the curve at point b is defined as a . The coefficients for mechanical stimulation and laser stimulation respectively, are shown in Table 3.3.

Table 3.3: Coefficients for the sigmoidal curve for mechanical and laser stimulation. a is the slope coefficient and b is the threshold of perceiving one or two points.

| Coefficients | Laser stimulation | Mechanical stimulation |
|--------------|-------------------|------------------------|
| a | 0.030932 | 0.218036 |
| b | 70.306153 mm | 31.470384 mm |

Learning algorithm

The aim of the learning algorithm was to train the model to predict the output, which is the spatial distribution of two simultaneously applied stimulations, and the probability of perceiving one or two points, for point-to-point distance between 10 mm and 100 mm, for laser and mechanical stimulation. This was achieved by training the model such that an excitatory weight vector w_e and inhibitory weight vector w_i , would provide the best generalized solutions for all point-to-point distances given a stimulation modality. The model was trained toward acquiring an amplitude of the separation point y equal to the probability of the stimulation being perceived as one or two points. The separation point was the point where the two stimulations would be separated on in the spatial distribution.

The lateral inhibition model was implemented with $R_1 = 1$ and $R_2 = 5$ (cf. Table 3.2). By applying the same R_1 and R_2 for all point-to-point distances, a gap of zeros would occur. An example of this is illustrated on Figure 3.7 where two laser stimulations with a point-to-point distance of 100 mm, $R_1 = 1$, and $R_2 = 5$ leaves a gap of zeros. The separation point at the center of the gap is highlighted.

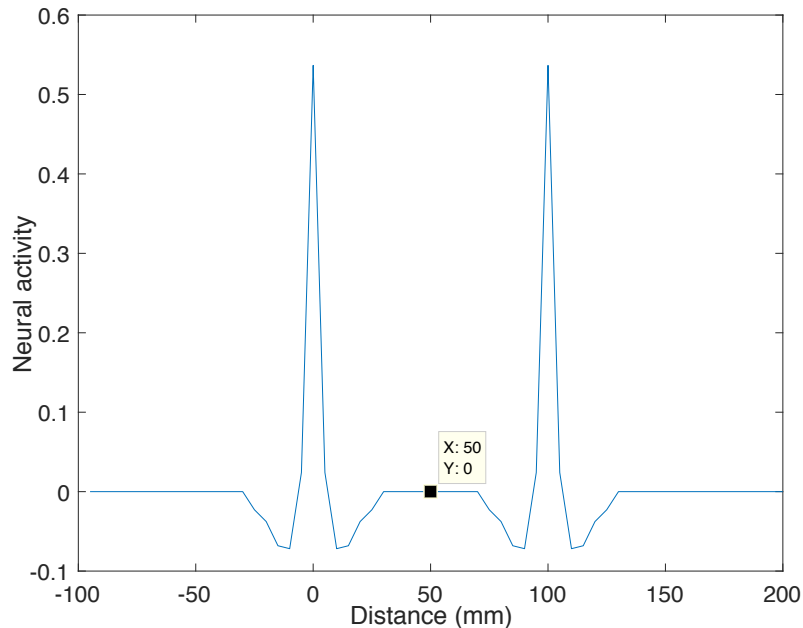


Figure 3.7: Two applied laser stimulations, with a point-to-point distance of 100 mm. Radius of region $R_1 = 1$, and $R_2 = 5$ leaving a gap of zeros. Thereby the separation point is zero.

Since the purpose of the training was to obtain a separation point equal to the probability of the stimulation being perceived as one or two points, it would not be feasible to have

a the amplitude of the starting value equal to zero. The reason being that no excitatory or inhibitory weight different from zero would be possible to achieve. Before initiating training R_1 and R_2 were increased by one for a point-to-point distance of 100 mm until a nonzero separation point was achieved. The new R_1 and R_2 were then applied for all point-to-point distances less than 100 mm. The optimal R_1 and R_2 for laser stimulation and mechanical stimulation are shown in Table 3.4. Figure 3.8 illustrates the result after applying the optimal radius of region $R_1 = 6$ and $R_2 = 10$ with a point-to-point distance of 100 mm for laser stimulation.

Table 3.4: Radius of region leaving a nonzero separation point for laser stimulation and mechanical stimulation.

| Radius of region | Laser stimulation | Mechanical stimulation |
|------------------|-------------------|------------------------|
| R_1 | 6 | 16 |
| R_2 | 10 | 20 |

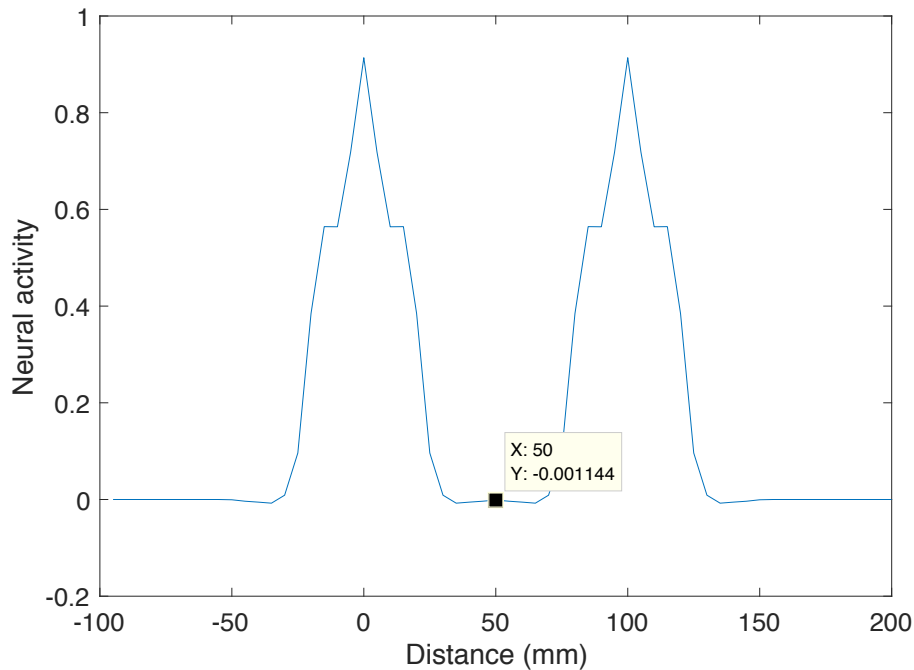


Figure 3.8: Two applied laser stimulations, with a point-to-point distance of 100 mm. Increasing the radius of region such that $R_1 = 6$, and $R_2 = 10$ leaves a nonzero gap. Thereby the separation point is nonzero.

Increasing R_1 and R_2 resulted in wider peaks removing the zero gap, while obtaining a separation point of -0.001144 before initializing the training. The model was trained using the optimal R_1 and R_2 , presented in Table 3.4. The training data t was the probability of the stimuli being perceived as one or two stimulations (cf. Section 3.1) for a point-to-point distance ranging from 10 mm to 100 mm with a step size of 1 mm. The reason for starting at 10 mm was to avoid extrapolation since the experimental data used a minimum point-to-point distance of 10 mm. The model training was performed with 10 different seeds of initial random excitatory and inhibitory weights.

The Gradient descent method was used as learning algorithm, which aims to obtain a w_e and w_i that results in the lowest total sum of squares error (SSE). [da Silva et al., 2017] The Gradient descent method uses the Delta rule to tune the randomly generated excitatory and inhibitory weights (cf. Section 3.3), in order to provide the best generalized solutions for all point-to-point distances for a given stimulation [da Silva et al., 2017]. The Delta rule minimizes SSE between t and the response from the model y at the current point-to-point distance. This resulted in 91 SSEs, one for each point-to-point distance that were used to update w_e , and w_i after, and used in calculating a total SSE by a summation of all 91 SSEs.

Due to the Gradient descent method updating w_e and w_i and minimizing the total SSE through iteration a, stop criteria must be implemented, otherwise the Gradient descent method would keep iterating. If the change in total SSE was less than 0.00001 or the total SSE increased compared to the previous iteration to the current iteration then the training would be stopped.

In the following the implementation of Gradient descent method for a single iteration is explained. Every activated neuron x_i in the input layer was set to 1 and the randomly generated excitatory weights w_e and inhibitory weights w_i were applied, where a symmetrical decay and rise with the lowest amplitude being at the center were achieved. Thereby an excitatory layer and an inhibitory layer were created and the output layer was then achieved by summation of the excitatory and inhibitory layer. This applied to all point-to-point distances. An example of the process with two laser stimulations is illustrated in Figure 3.9.

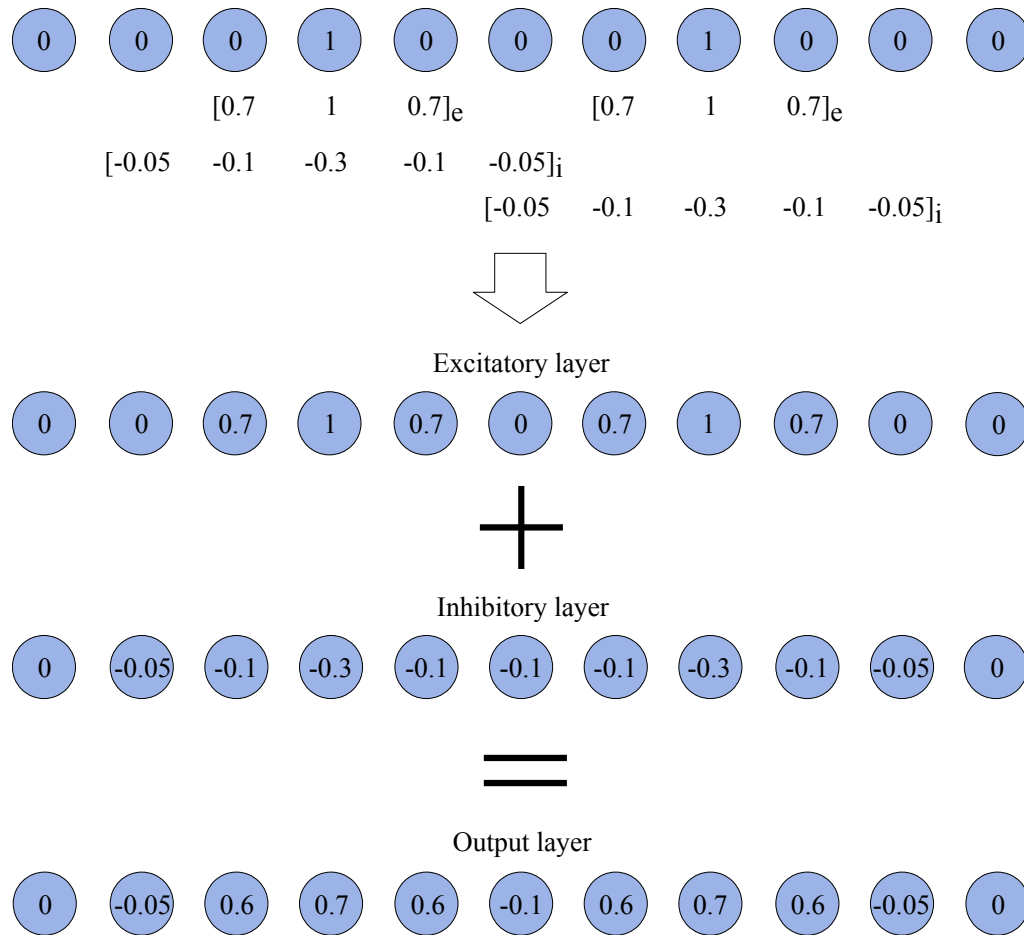


Figure 3.9: Two neurons are activated where a set of excitatory weights [...]e and inhibitory weights [...]i are applied at each stimulation. Symmetrical decay occurs from the center of the stimulation for the excitatory weights, while symmetrical increase occurs from the center of the stimulation for the inhibitory weights. The output layer consists of the summation between the excitatory and inhibitory layer.

The following procedure was performed for each point-to-point distance. The separation point which is the center of the gap between the two stimulations was extracted and used to calculate the SSE [da Silva et al., 2017]:

$$SSE = \frac{1}{2} \cdot (t - y)^2 \quad (3.7)$$

The SSE in equation (3.7) can be expressed as [da Silva et al., 2017]:

$$SSE = \frac{1}{2} \cdot (t - (x_i \cdot w_e + x_i \cdot w_i))^2 \quad (3.8)$$

The gradients are calculated in order to know which direction the weights must be altered such that SSE is minimized [da Silva et al., 2017]:

$$\nabla SSE_e = \frac{\partial SSE}{\partial w_e} \quad (3.9)$$

$$\nabla SSE_i = \frac{\partial SSE}{\partial w_i} \quad (3.10)$$

The gradient that minimizes SSE is calculated as following and used during the weight update [da Silva et al., 2017]:

$$\nabla SSE_e = -(t - y) \cdot x_i \quad (3.11)$$

$$\nabla SSE_i = -(t - y) \cdot x_i \quad (3.12)$$

Since in this case $\nabla SSE_e = \nabla SSE_i$ one ∇SSE can be used for updating both w_e and w_i .

The variation Δw for updating the w_e and w_i is given by [da Silva et al., 2017]:

$$\Delta w = -\eta \cdot \nabla SSE \quad (3.13)$$

where η is the learning rate determining the step size at which the learning algorithm moves with towards the minimal SSE. The learning rate is typically between 0 and 1, where the model is chosen to be trained with a learning rate of 0.01. Since the aim is to minimize SSE, the weight update is done in opposite direction of the gradient and therefore resulting in Δw being negative. [da Silva et al., 2017] By substituting equation (3.11) in equation (3.13), an expression of equation (3.13) is obtained [da Silva et al., 2017]:

$$\Delta w = \eta \cdot (t - y) \cdot x_i \quad (3.14)$$

The update of the excitatory weight and inhibitory weight is then calculated by [da Silva et al., 2017]:

$$w_{e,updated} = w_{e,previous} + \eta \cdot (t - y) \cdot x_i \quad (3.15)$$

$$w_{i,updated} = w_{i,previous} + \eta \cdot (t - y) \cdot x_i \quad (3.16)$$

A geometric interpretation of the Delta rule is illustrated in Figure 3.10.

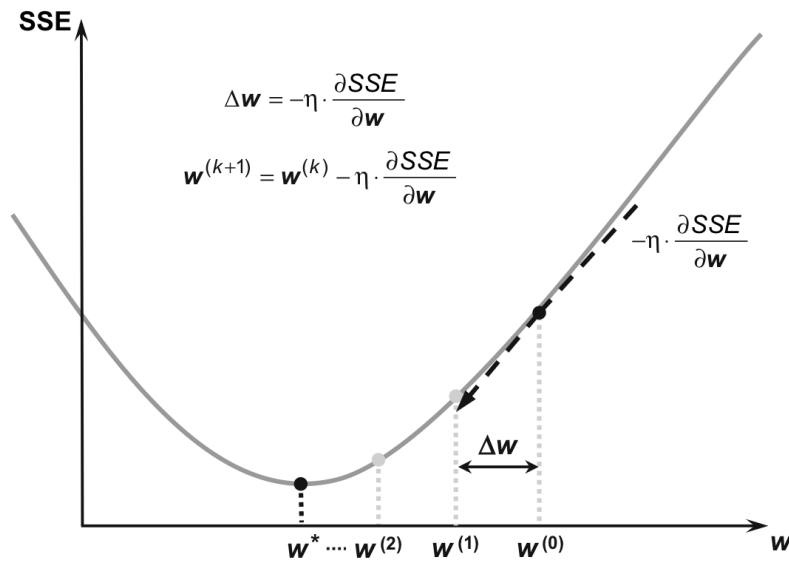


Figure 3.10: Geometrical interpretation of the delta rule. The weights are updated from the initial $w^{(0)}$ toward $w^{(*)}$ which is the point of convergence where SSE is minimal. The next value of $w^{(1)}$ is obtained by updating the weight in the opposite direction of the gradient Δw with respect to $w^{(0)}$. This is repeated for $w^{(k)}$ until point of convergence $w^{(*)}$ is achieved. This applies for both w_e and w_i . [da Silva et al., 2017] Adapted from: da Silva et al. [2017]

During the weight update the Gradient descent method would allow for w_e to assume negative values and w_i positive values. To ensure a lateral inhibition model approaching biological reality and avoid overfitting, constrains were implemented ensuring that w_e was always positive, and w_i always negative. The following constrain was implemented for w_e :

```

if  $w_{e,updated} > 0$ 
     $w_e = w_{e,updated}$ 
else
     $w_e = w_{e,previous}$ 

```

The following constrain was implemented for w_e :

```

if  $w_{i,updated} < 0$ 
     $w_i = w_{i,updated}$ 
else
     $w_i = w_{i,previous}$ 

```

Moreover a second constrain was implemented with regard to maintaining symmetrically decay for w_e , and a symmetrically rise for w_i . If the preceding weight was lower or equal to the updated weight then w_e was changed to equal a random weight lower than the preceding weight and higher than the upcoming weight:

```

if  $w_{e,previous} \leq w_{e,updated}$ 
     $w_e = w_{e,random}$     satisfying  $w_{e,updated} > w_{e,random} > w_{e,next}$ 
else
     $w_e = w_{e,updated}$ 

```

If the preceding weight was higher or equal to the updated weight then w_i was changed such that it would be equal to a random weight higher than the preceding weight and lower than the upcoming weight:

```

if  $w_{i,previous} \geq w_{i,updated}$ 
     $w_i = w_e = w_{e,random}$     satisfying  $w_{e,updated} < w_{e,random} < w_{e,next}$ 
else
     $w_i = w_{i,updated}$ 

```

After updating w_e and w_i with the Gradient descent method and constrains at every point-to-point distance, the Total SSE was calculated:

$$Total\ SSE = \sum SSE \quad (3.17)$$

Lastly the Gradient Descent method would test if the stop criteria are met. If they were then the update of w_e and w_i would be stopped, else it would run another iteration. After a number of iterations the total SSE would decrease and remain constant at the minimal total SSE. The response of the total SSE with respect to the number of iterations is described as a decreasing curve as illustrated in Figure 3.11.

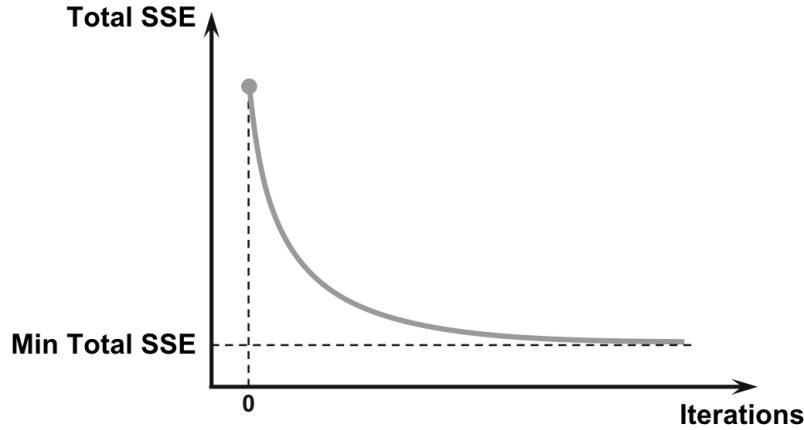


Figure 3.11: The response of the total SSE as the number of iterations increase. The total SSE decreases until it reaches a minimum at which it will remain. Adapted from da Silva et al. [2017].

The R_1 and R_2 found to be optimal and presented in Table 3.4 does not necessarily provide a trained lateral inhibition model for both modalities with the highest prediction accuracy. Therefore an algorithm is implemented in order to determine a set of R_1 and R_2 for each modality, which the model is trained with, results in the highest prediction accuracy. The

initial R_1 and R_2 values was the optimal values and the algorithm increased both R_1 and R_2 , with the constrain of $R_2 > R_1$ and the maximum value of R_1 and R_2 to be 30. The algorithm calculates the prediction accuracy with all set combinations of R_1 and R_2 , where the set that resulted in the highest prediction accuracy was chosen during model training to acquire w_e and w_i . Thereby the aim is to acquire a lateral inhibition model for each modality that fits the training data.

Several methods exist to evaluate the prediction accuracy of a model. Two known methods are the Mean square error (MSE) and Mean absolute error (MAE). MSE is calculated by [Wallach and Goffinet, 1989]:

$$MSE = \frac{1}{n} \sum_{i=1}^n (y - t)^2 \quad (3.18)$$

where y is model output and t is the training data. MAE is calculated by following [Chai and Draxler, 2014]:

$$MAE = \frac{1}{n} \sum_{i=1}^n |y - t| \quad (3.19)$$

As apparent from equation (3.18) and equation (3.19) the main difference MSE and MAE lies in MSE squaring the error, while MAE uses the absolute value of the error. There is the possibility of having outliers between the model and the training data. Using MSE the weighting of these outliers would be increased due to squaring the error, which is undesirable for evaluating the overall performance of the model. However this is avoided by using MAE as the weighting to each error is equal. Therefore MAE will be used to calculate the prediction accuracy, where a MAE equal to 0 corresponds to 100 % prediction accuracy. [Wallach and Goffinet, 1989; Chai and Draxler, 2014]

A flowchart of the model training with the implementation of the Gradient Descent method with constrains and the optimization algorithm for R_1 and R_2 is illustrated in Figure 3.12.

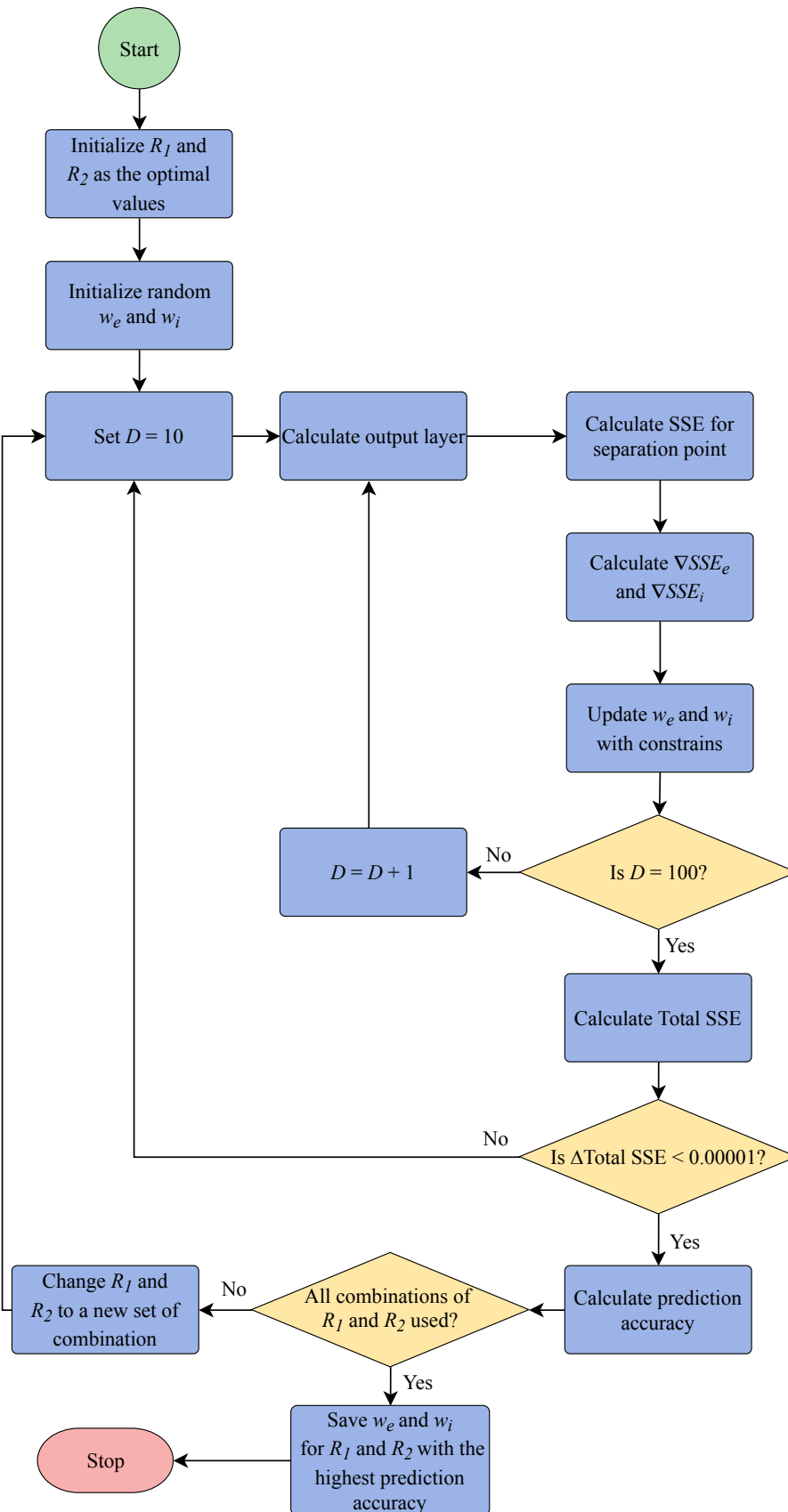


Figure 3.12: Flowchart of the model training implemented with the Gradient Descent method as learning algorithm. The model is trained for all set of combinations of R_1 and R_2 to determine the set that results in the highest prediction accuracy.

3.5 Data analysis

In the following the methods used to analyze model output and training are explained. The spatial distribution of the output after applying a ramp activation function will be presented for laser and mechanical stimulation for a single seed. Following this the rest of the data analysis will be based on 10 random seeds of model training for both laser stimulation and mechanical stimulation. The excitatory weights and inhibitory weights are extracted prior to applying the ramp activation function in order to analyze their characteristics with regard to biology i.e. the excitatory weights having a symmetrical decay and the inhibitory weights having symmetrical rise, and to determine if the weights differ considerably after training with the Gradient Descent method for every random seed. Moreover the response of the total SSE as the number of iterations increase is evaluated. Ideally the response of the total SSE should look similar to Figure 3.11, which illustrates a decrease in total SSE as the number of iterations are increased.

A direct comparison of the two-point discrimination threshold between the model and training data provided by Frahm et al. [2017] is performed, and fitted sigmoidal curves of both model output and training data are used for comparison of the probability of perceiving one or two stimulations for different point-to-point distances. It is of interest to determine the performance of the model, why comparison of two-point discrimination data based on limits of agreement is conducted with a Bland-Altman plot presented by Altman and Bland [1983]. The Bland-Altman plot compares the agreement between two different methods [Altman and Bland, 1983]. The Bland-Altman plot shows 95 % limits of agreement, and confidence intervals (CI) for the mean bias and for the limits of agreement, which is the basis for analyzing the relationship between the difference and the magnitude of measurement. [Altman and Bland, 1999] 95 % of the differences must be found within the limits of agreement, which is defined by:

$$\text{Limits of agreement} = d \pm 1.96SD \quad (3.20)$$

where d is the mean bias of the differences and SD is the standard deviation of the differences between the two methods. [Altman and Bland, 1999] For the Bland-Altman plot it is required of the difference between the methods to be normally distributed. Although having non-normally distributed difference causes no great impact upon estimating limits of agreement. [Altman and Bland, 1999] In the case of having non-normally distributed and having one or more extreme discrepancies between the methods a nonparametric approach preferable Altman and Bland [1999]. The nonparametric approach is generally less reliable, than the parametric approach, particularly in small samples [Altman and Bland, 1999]. Since the sample size of the model output and training data is small and there is no extreme discrepancies between the methods, the parametric approach is used.

3.6 Sensitivity analysis

A sensitivity analysis is conducted for the purpose of achieving a better understanding of how sensitive the output of the model is to a particular input. The sensitivity analysis for a model is conducted by adjusting the input parameters from their minimum to maximum

values. Thereafter the model's sensitivity to a specific input can be determined as the amount of change in the model output. [Negnevitsky, 2005]

The sensitivity analysis for the lateral inhibition model is performed to inspect the sensitivity of the model to D for each modality with and without shifting the stimulation (cf. Section 3.3). The purpose of the sensitivity analysis was therefore to investigate how the probability of perceiving one or two points for point-to-point distances between 10 mm and 100 mm changes after adjusting D with ± 0.5 mm with and without shifting the stimulation. The sensitivity analysis is performed on a single seed of the lateral inhibition model for each modality.

3.7 Model validation

The predictive performance of the model with regard to predicting two-point discrimination for laser and mechanical stimulation can be achieved by comparing the accuracy of the model output to the training data. MAE is chosen as the preferred method to evaluate the overall performance of the model. This is due to MAE weighting the errors equally compared to MSE which squares the error (cf. Section 3.4)

The model is also validated by a using two-point discrimination data from literature. If the data had been fitted the two-point discrimination data from 10 mm to 100 mm it would be extracted and used for for model validation. If there was no fit only the two-point discrimination threshold was used during model validation. Literature included two-point discrimination and gap-detection data, along with data from different stimulation sites such as the forearm, hand or finger. Table 3.5 and Table 3.6. shows the studies used for validating the model for laser and mechanical stimulation respectively.

Table 3.5: Two-point discrimination data for laser stimulation used in the model validation.

| Study | Stimulation diameter | Threshold | Stimulation area | Stimulation type |
|-------------------------|----------------------|-----------|--------------------------------|------------------|
| Mørch et al. [2010] | 5 mm | 58.9 mm | Forearm | Laser |
| Mørch et al. [2010] | 5 mm | 44.3 mm | Abdomen | Laser |
| Schlereth et al. [2001] | 5 mm | 6.7 mm | Hand dorsum Radial-ulnar | Laser |
| Schlereth et al. [2001] | 5 mm | 11.1 mm | Hand dorsum Proximal-distal | Laser |

Table 3.6: Two-point discrimination data for mechanical stimulation used in the model validation.

| Study | Stimulation diameter | Threshold | Stimulation area | Stimulation type |
|--------------------------------------|-----------------------------|------------------|--------------------------------|-------------------------|
| Mørch et al. [2010] | 0.5 mm | 35 mm | Forearm | Pressure |
| Mørch et al. [2010] | 5 mm | 20.3 mm | Abdomen | Pressure |
| Schlereth et al. [2001] | 1.1 mm | 7.8 mm | Hand dorsum Radial-ulnar | Pressure |
| Schlereth et al. [2001] | 1.1 mm | 10.4 mm | Hand dorsum Proximal-distal | Pressure |
| Lévêque et al. [2000] | 5 mm | 23.3 mm | Left forearm | Pressure |
| Lévêque et al. [2000] | 5 mm | 24.3 mm | Right forearm | Pressure |
| Johnson and Phillips [1981] | 2 mm | 0.87 mm | Finger | Pressure |
| Martikainen and Pertovaara [2002] | 6 mm | 17.3 mm | Forearm | Pressure |

For both Table 3.5 and Table 3.6, the study by Mørch et al. [2010] was the only one with data fitted to a sigmoidal curve. Therefore MAE was calculated for the study by Mørch et al. [2010] and absolute error of the two-point discrimination threshold for the rest.

Results 4

In this chapter the results of the data analysis, sensitivity analysis and model validation is presented.

4.1 Model output

The model was trained using the Gradient descent method, which aimed to minimize the total SSE at each point-to-point distance and obtain a set of excitatory and inhibitory weights. The radius of the excitatory field, R_1 , and inhibitory field, R_2 , that was used during model training, which gave the highest prediction accuracy, is presented in Table 4.1.

Table 4.1: Radius of the excitatory field and inhibitory field that after training resulted in the highest prediction accuracy for each modality.

| Radius of region | Laser stimulation | Mechanical stimulation |
|------------------|-------------------|------------------------|
| R_1 | 16 | 16 |
| R_2 | 20 | 20 |

The results for laser stimulation using the initial optimal weights $R_1 = 6$ and $R_2 = 10$ are shown in Appendix D. They show that the lateral inhibition model was trained poorly for laser stimulation why R_1 and R_2 were further optimized after closing the zero gap.

The response of the total SSE per iteration for 10 seeds calculated during model training is shown in Figure 4.1. Figure 4.1a shows the obtained total SSE per iteration from 10 laser stimulation seeds. The total SSE for laser stimulation show a decline for all seeds until it reaches a minimum as the number of iterations are increased. Figure 4.1b shows the total SSE from 10 mechanical stimulation seeds where the total SSE decreases until a minimum is reached.

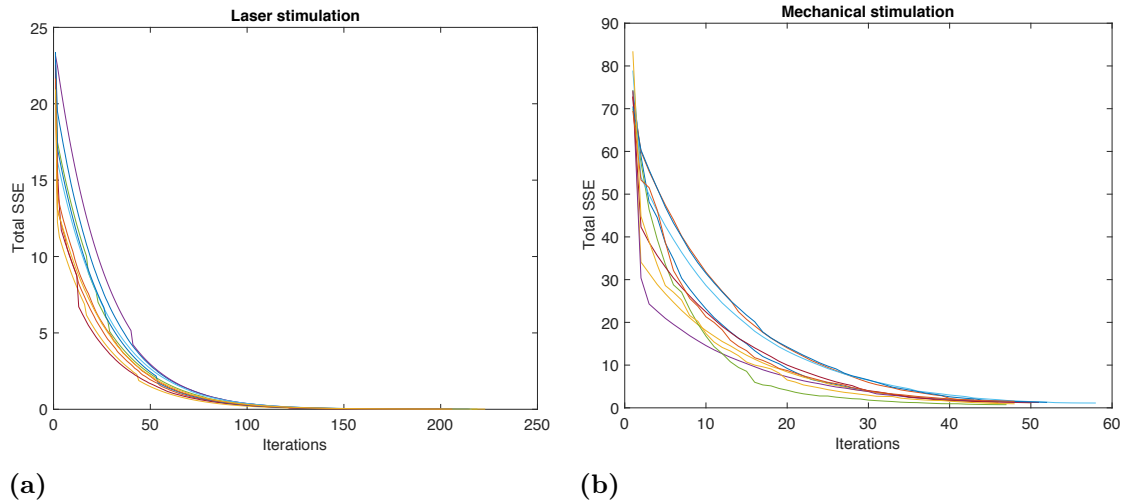


Figure 4.1: Response of the total SSE of 10 seeds for (a) laser stimulation and (b) mechanical stimulation as the number iterations increase.

To analyze the characteristics of the excitatory and inhibitory weights with regard to biological reality the weights vectors were extracted for 10 seeds, after model training. Moreover, the summation of the weight vectors were plotted to determine if they had they had Mexican-hat shape. The weights summation thereof are shown in Figure 4.2, where the figures on the left are for laser stimulation, and those on the right for mechanical stimulation. The excitatory weights for both modalities showed symmetrical decay from stimulation center, while the inhibitory weights show symmetrical rise from the stimulation center. The summated weights show a Mexican hat shape. Figure 4.2e and 4.2f shows weak negative connection strength in the extremities of the distance caused by the inhibitory weight vector, though still with the characteristics of the Mexican-hat function.

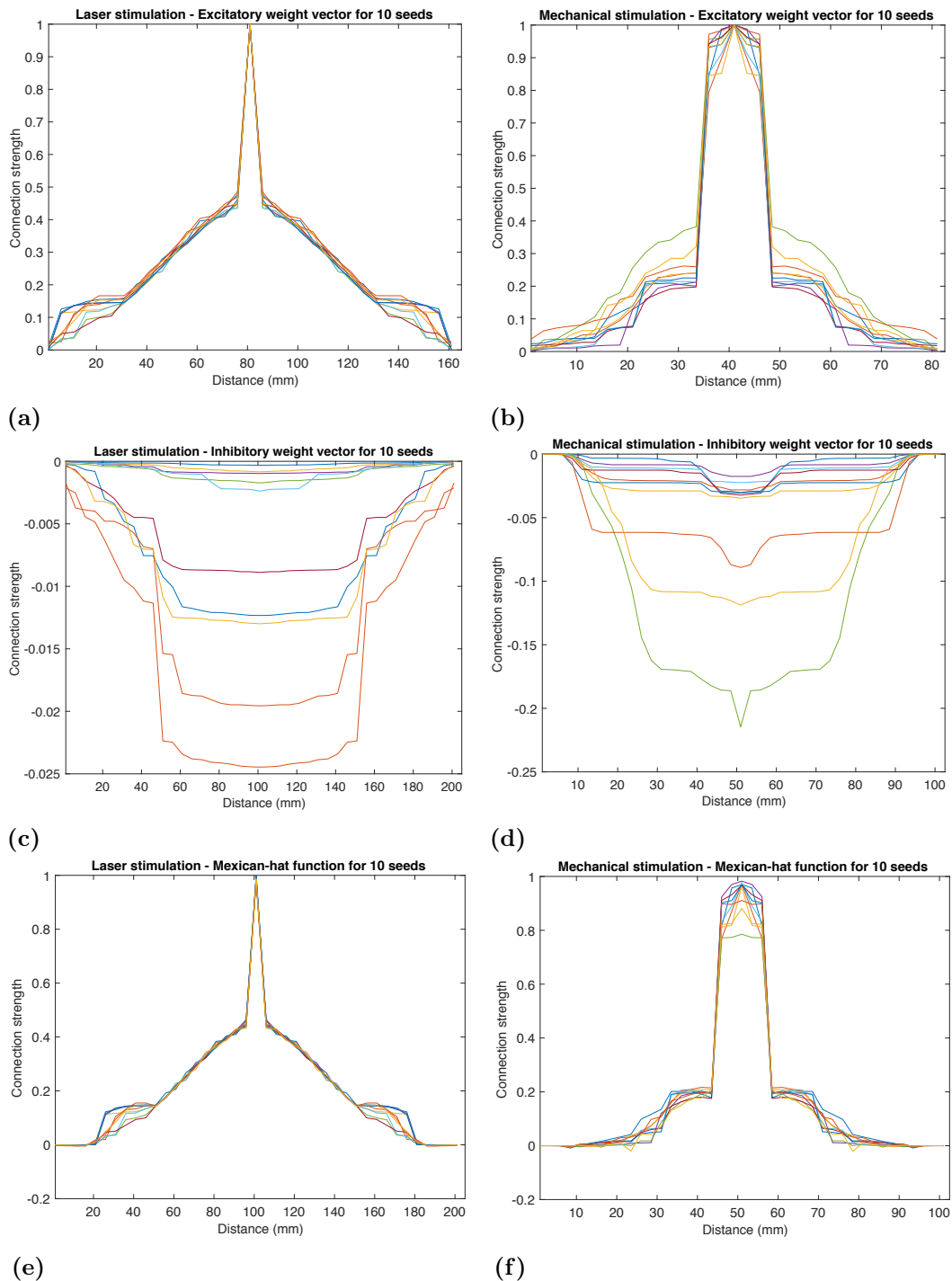
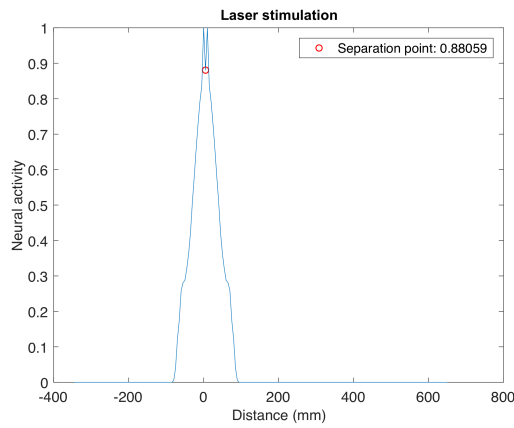
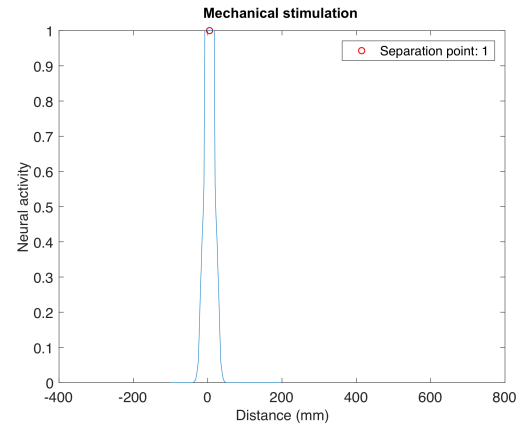


Figure 4.2: The weight vectors of 10 seeds, after model training for laser and mechanical stimulation. The left side show the weights for laser stimulation where (a) show the excitatory and (c) show the inhibitory weights. The right side show the weights for mechanical stimulation where (b) show the excitatory and (d) show the inhibitory weights. (e) and (f) shows the summation of the excitatory and inhibitory weights for the ten seeds after model training, for laser and mechanical stimulation respectively. The x-axis is the element in the weight vector, while the y-axis shows the connection strength. Symmetrical decay is present for the excitatory weight, while symmetrical rise is present for the inhibitory weights. The summations show a Mexican-hat like shape.

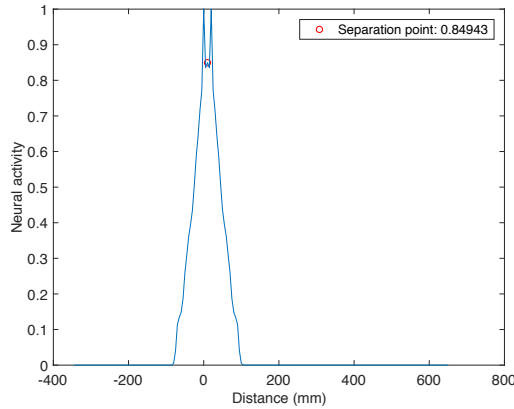
The responses of two-point discrimination were achieved based on the excitatory and inhibitory weights and are visualized as a spatial distribution of the stimulation for laser and mechanical stimulation for a point-to-point-distance changing from 10 mm to 100 mm with a step of 10 mm as presented in Figure 4.3. The spatial distribution was achieved after applying a ramp activation function (cf. Equation 3.4 in Section 3.3) in the range of $[0, 1]$. A red circle indicates the separation point along with its amplitude corresponding to the probability perceiving two stimulations as one or two points.



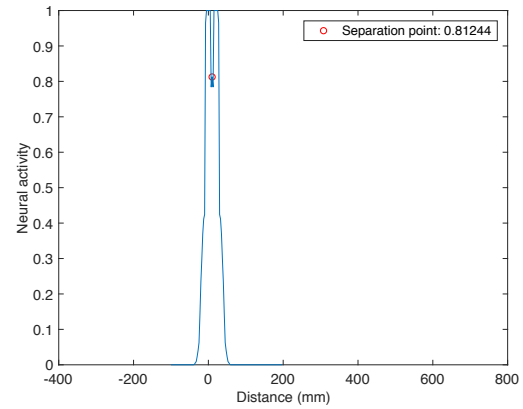
(a) Point-to-point distance of 10 mm



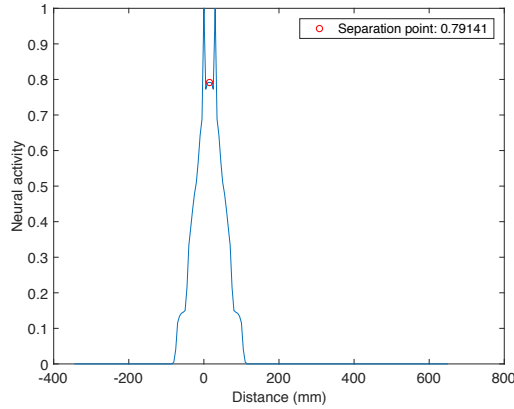
(b) Point-to-point distance of 10 mm



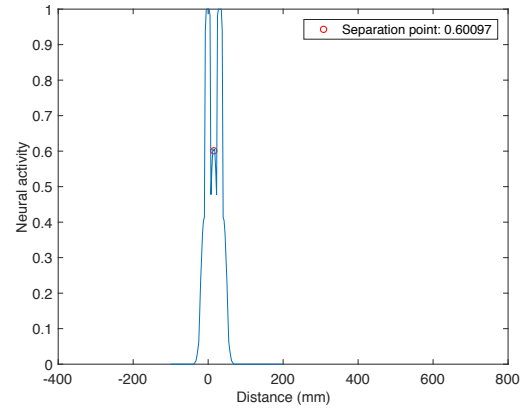
(c) Point-to-point distance of 20 mm



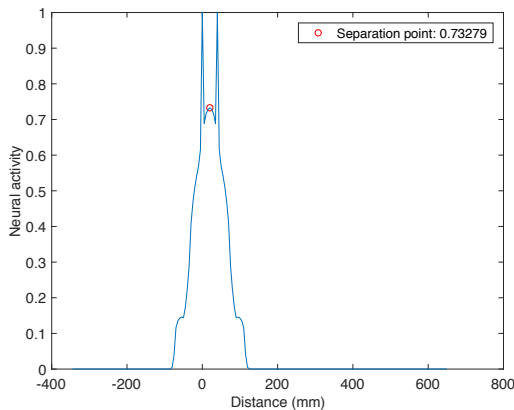
(d) Point-to-point distance of 20 mm



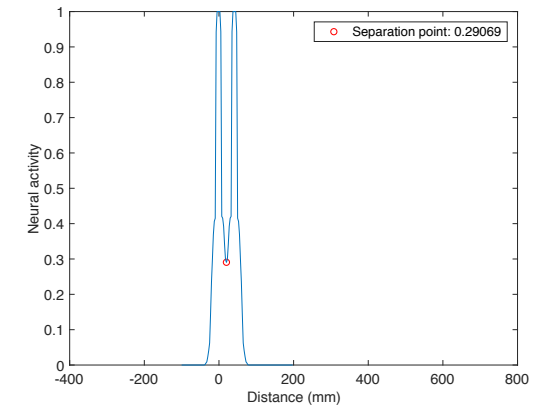
(e) Point-to-point distance of 30 mm



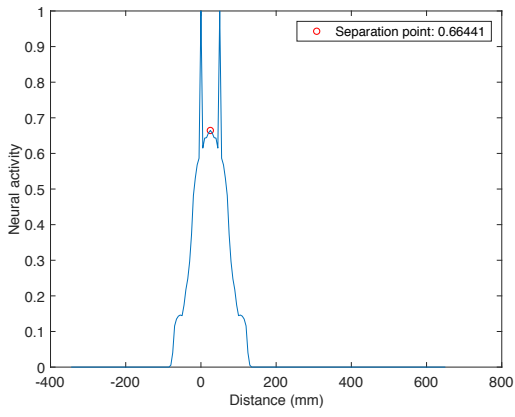
(f) Point-to-point distance of 30 mm



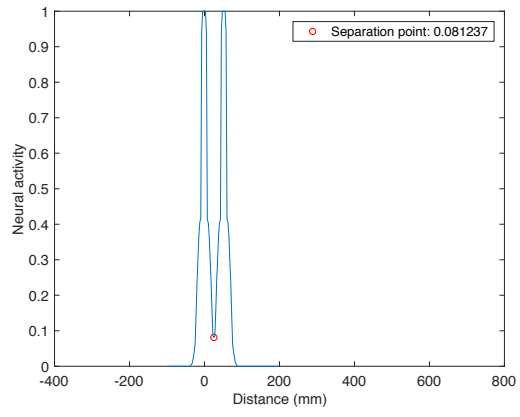
(g) Point-to-point distance of 40 mm



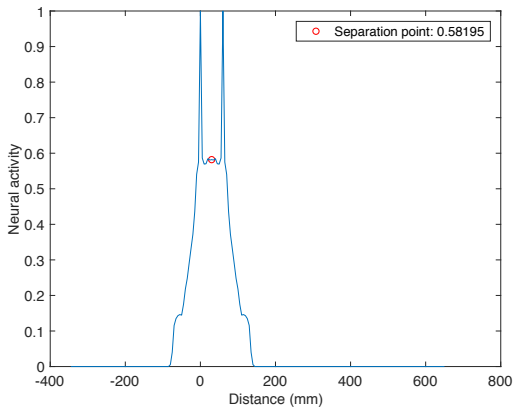
(h) Point-to-point distance of 40 mm



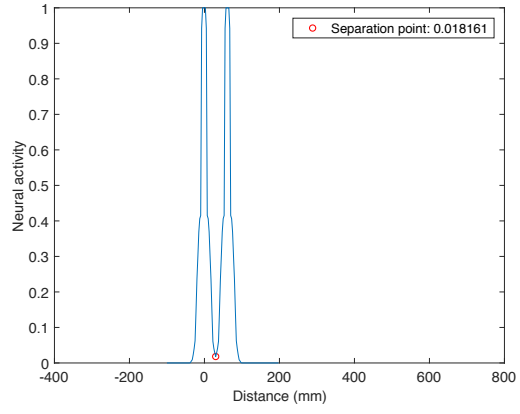
(i) Point-to-point distance of 50 mm



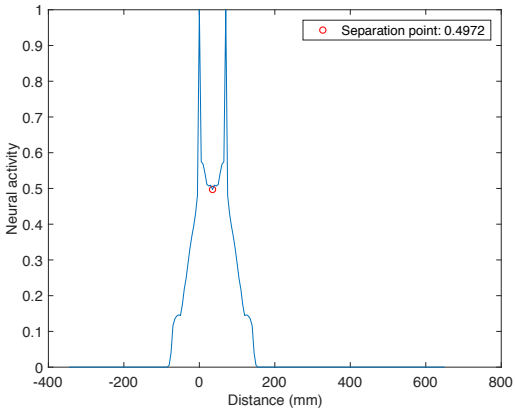
(j) Point-to-point distance of 50 mm



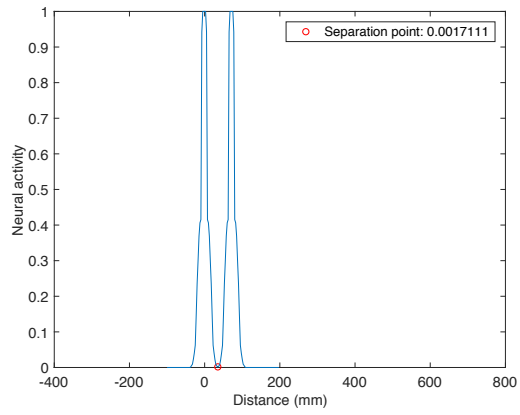
(k) Point-to-point distance of 60 mm



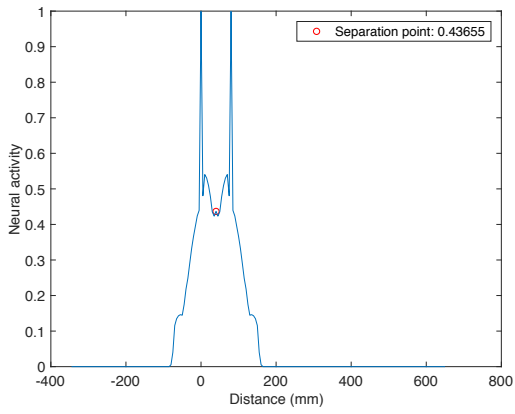
(l) Point-to-point distance of 60 mm



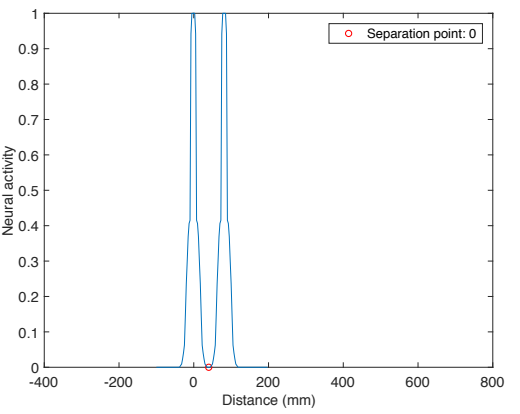
(m) Point-to-point distance of 70 mm



(n) Point-to-point distance of 70 mm



(o) Point-to-point distance of 80 mm



(p) Point-to-point distance of 80 mm

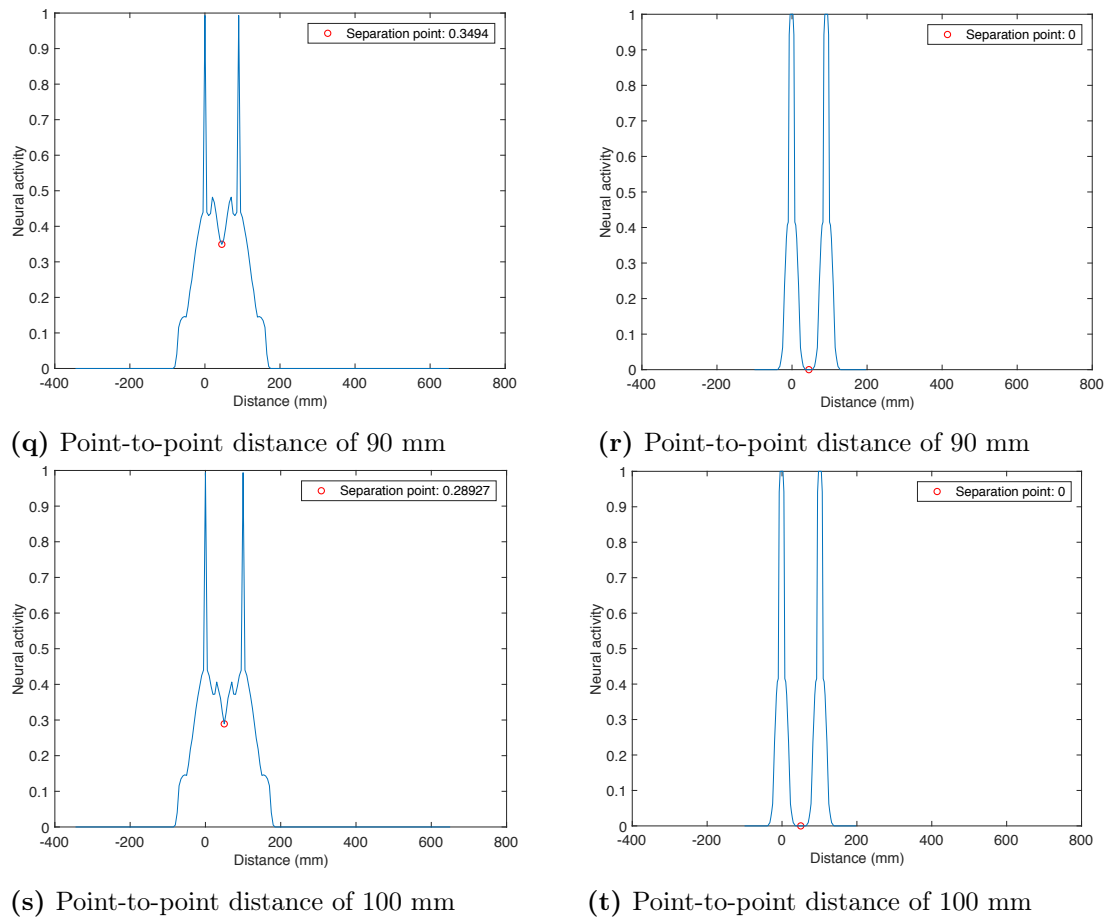


Figure 4.3: Spatial distribution over distances of 10 mm to 100 mm for laser stimulation (left) and mechanical stimulation (right), after applying the ramp activation function $[0, 1]$. The separation point is indicated by a red circle at each point-to-point distance.

To analyze the response to two-point discrimination from the laser and mechanical stimulations, the responses to the two-point discrimination for trained lateral inhibition model were plotted for 10 seeds at point-to-point distances from 10 mm and 100 mm, and are shown in Figure 4.4. Moreover the sigmoidal curve fitted from the training data which indicated by a thick blue line was plotted. The sigmoidal curves for laser and mechanical stimulation is shown in Figure 4.4a and Figure 4.4b respectively. The point where the dashed line intersects with the curves are the two-point discrimination threshold.

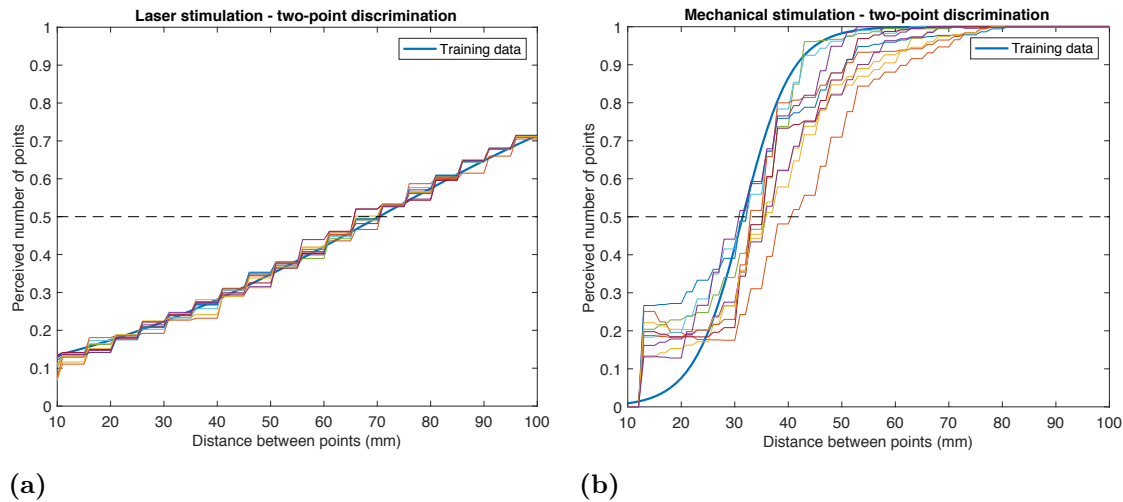


Figure 4.4: Probability of perceiving one or two points when changing the point-to-point distance between stimulations for (a) laser stimulation and (b) mechanical stimulation. Each plot shows 10 seeds per modality. The training data is shown in thick blue line and the dashed line indicates the 50 % threshold of perceiving one of two points.

For laser stimulation the two-point discrimination threshold for the training data is at 70.31 mm, while two-point discrimination threshold for the 10 seeds ranges between 65.66 mm and 70.55 mm. For mechanical stimulation the two-point discrimination threshold for the training data is at 31.47 mm while the two-point discrimination threshold for the 10 seeds ranges between 30.77 mm and 40.49 mm.

To analyze the agreement between model output and find where the model differs from the training data, Bland-Altman plots comparing the model output and training data for laser and mechanical stimulation were created and are shown in Figure 4.5a and Figure 4.5b respectively. Table 4.2 shows the mean bias and the standard deviation of differences, used for the 95 % limits of agreement estimation. In Figure 4.5 the upper and lower limits of agreement is illustrated by a dashed line, mean bias as a solid line, and 0 mean bias as a dash-dotted line. Each dot corresponds to the difference between the output of the lateral inhibition model and the training data as the probability of a stimulation to be perceived as two points. The x-axis show mean perceived number of points, where 0 corresponds to one point and 1 corresponds to two points.

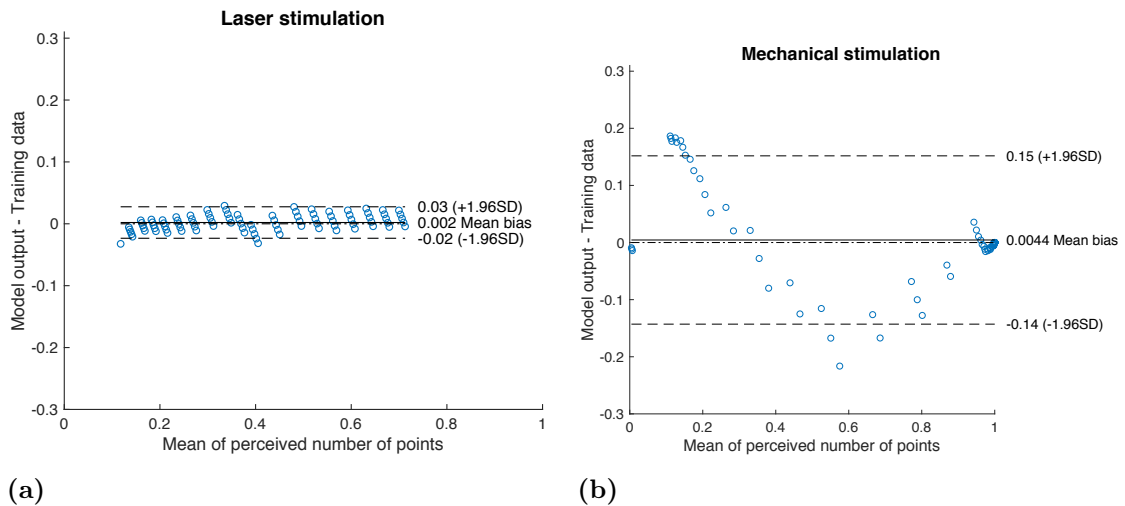


Figure 4.5: The Bland-Altman plot of the comparison between the model output and the training data for laser and mechanical stimulation. Each dot corresponds to the difference between the output of the lateral inhibition model and the training data as the probability of a stimulation to be perceived as two points. The Bland-Altman is presented a total of 91 points, one for each point-to-point distance from 10 mm to 100 mm with a step of 1 mm. The x-axis show mean perceived number of points, where 0 corresponds to one point and 1 corresponds to two points.

Table 4.2: The parameters used to calculate the confidence interval for the Bland-Altman plot of each modality.

| Parameter | Laser stimulation | Mechanical stimulation |
|-----------------------------------|--------------------|------------------------|
| Mean bias | 0.002 | 0.0044 |
| Standard deviation of differences | 0.0014 | 0.0079 |
| 95% Limits of agreement | from -0.02 to 0.03 | from -0.14 to 0.15 |

For laser stimulation based on the mean bias of 0.002 the model had minor differences between training data and model output. The limits of agreement were almost identical meaning that the data was symmetrically distributed around the mean bias. The model showed outliers when the probability of perceiving one or two points was 0.1 and 0.4. In general the model for laser stimulation agrees with the training data.

For the mechanical stimulation, based on the Bland-Altman plot in Figure 4.5b the difference between the output from the model output and the training data is minor, hence the mean bias of 0.0044. The limits of agreement were almost identical resulting in symmetrical distribution of the data around mean bias. The model showed outliers when the probability of perceiving one or two points was 0.1 and between 0.5 and 0.7. In the range of 0.1 and 0.3 the model overestimates the probability of perceiving one or two points, while it underestimates in the range of 0.3 and 0.9. In the range of 0.9 and 1 the model output and training data are almost identical.

4.2 Sensitivity analysis

A sensitivity analysis was conducted for both laser and mechanical stimulation to evaluate how sensitive the output of the model was to changes in the input parameters. The parameters changed were the receptive field diameter of nociceptors and tactile mechanoreceptors which were altered with ± 0.5 mm. The second parameter was shifting of the stimulation which would result in a change in the number of activated neurons. The results of the sensitivity analysis represented as by the two-point discrimination responses for point-to-point distances 10 mm to 100 mm and shown in Figure 4.6. The x-axis show the point-to-point distance between two stimulation with a 10 mm step. The y-axis show the perceived number of points for each receptive field diameter. The two-point discrimination threshold is given by the point where two-point discrimination response and the dashed line intersect.

The results of the sensitivity analysis are represented by the two-point discrimination responses for point-to-point distances 10 mm to 100 mm and shown in Figure 4.6. The x-axis show the point-to-point distance between two stimulation with a 10 mm step. The y-axis show the perceived number of points for each receptive field diameter. The two-point discrimination threshold is given by the point where two-point discrimination response and the dashed line intersect.

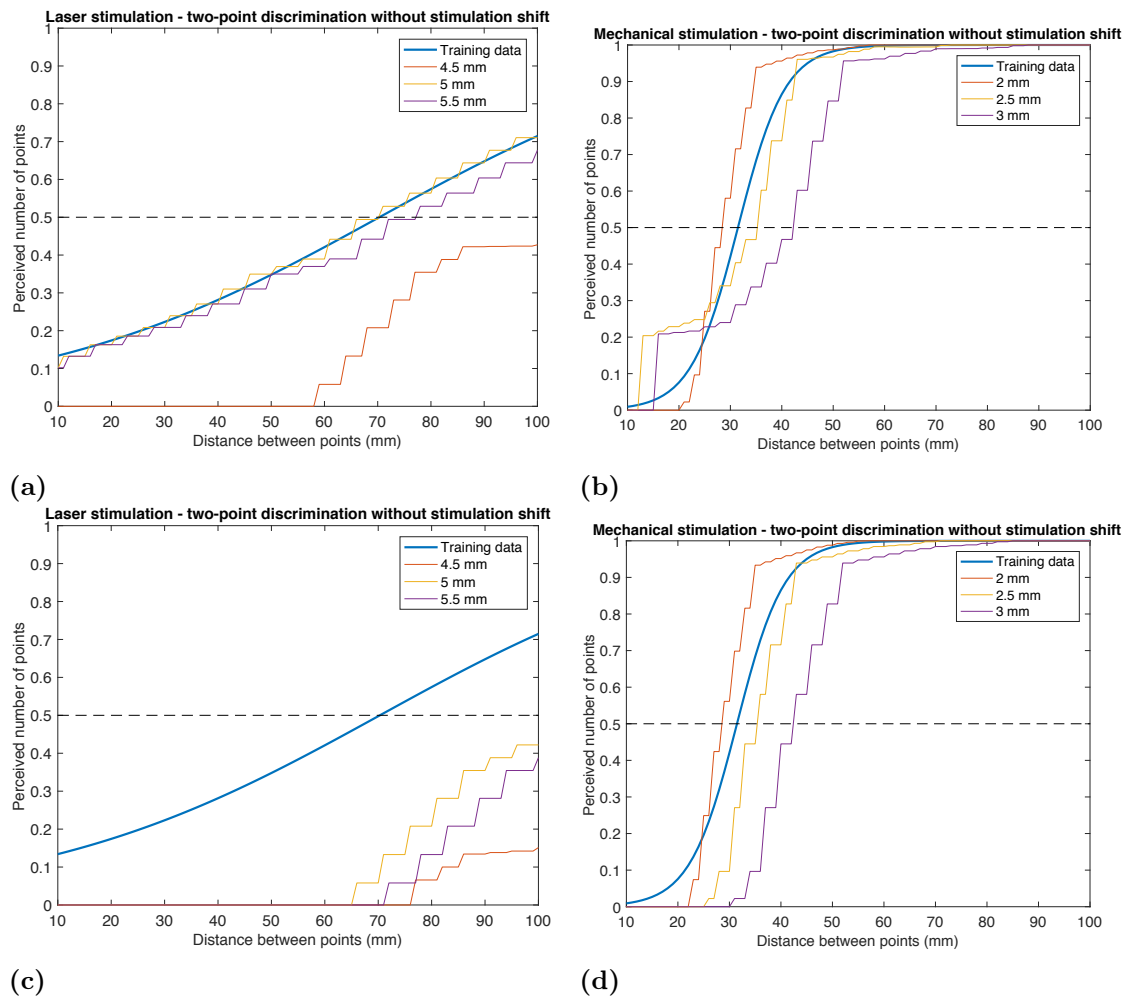


Figure 4.6: Sigmoidal representation of the sensitivity analysis performed for laser and mechanical stimulation, with and without stimulation shift. (a) Laser stimulation without stimulation shift. (b) Laser stimulation with stimulation shift. (c) Mechanical stimulation without stimulation shift. (d) Mechanical stimulation with stimulation shift. The x-axis is the point-to-point distance between 10 mm and 100 mm for every tenth distance, while the y-axis is the perceived number of points. The intersection between the dashed line and the graph indicates the two-point discrimination threshold.

For laser stimulation the lateral inhibition model was originally designed using a receptive field diameter of 5 mm. The sensitivity analysis showed that decreasing the receptive field diameter to 4.5 mm resulted in the model being more prone to underestimating the probability of perceiving one or two points at all point-to-point distances compared to 5 mm. Increasing the receptive field diameter to 5.5 mm resulted in model underestimating probability of perceiving one or two points slightly compared to 5 mm. As shown on Figure 4.6a the lateral inhibition model using a receptive diameter of 5.5 mm has many similarities to the training data, while that of 4.5 mm has no similarities at all. Stimulation shift for all receptive field diameters including 5 mm resulted in the lateral inhibition model being completely different from the training data as shown in Figure 4.6c.

For mechanical stimulation the model was originally designed using a receptive field

diameter of 2.5 mm. The sensitivity analysis showed that decreasing the receptive field diameter to 2 mm resulted in the model underestimating the probability of perceiving one or two points at a point-to-point distance of 20 mm compared to 2.5 mm as shown on Figure 4.6b. However at point-to-point distances of 10 mm and 20 mm the model no longer overestimates the probability of perceiving one or two points when comparing to it to the training data as was the case for 5 mm. Increasing the receptive field diameter to 3 mm resulted in the model underestimating the probability of perceiving one or two points compared to both the training data and receptive field diameter of 2.5 mm. At point-to-point distances of 10 mm and 20 mm the model would still overestimate probability of perceiving one or two points as was the case with 2.5 mm.

Shifting the stimulation had no major impact for a receptive field diameter of 2 mm compared to 2.5 mm as shown Figure 4.6d. However it did cause the model to become more similar to the training data. For a receptive field of 2.5 mm the model no longer overestimated the probability of perceiving one or two points at point-to-point distances 10 mm and 20 mm when shifting the stimulation. It did however deviate slightly from the training data. For the receptive field diameter of both 3 mm the model no longer overestimated the probability of perceiving one or two points at point-to-point distances 10 mm and 20 mm when shifting the stimulation, as was the case with 2.5 mm though it would still underestimate compared to both 2.5 mm and the training data.

Overall the model performed well in predicting the probability of perceiving one or two points. What was noticeable for receptive field diameter of 2.5 mm was that the estimations at point-to-point distances 10 mm and 20 mm also seemed to have been corrected by shifting the stimulation, making it more similar to the training data.

4.3 Model validation

The validation of the model was done with regard to determining the prediction accuracy for the lateral inhibition model for laser stimulation and mechanical stimulation. The models prediction accuracy compared to the training data for both modalities was evaluated by calculating the MAE. Training of the lateral inhibition model was performed on 10 seeds for each stimulation modality used to calculate a MAE thereof. The calculated MAE of the lateral inhibition model for both modalities are shown in Table 4.3.

Table 4.3: Prediction accuracy of the lateral inhibition model evaluated using MAE. The MAE was calculated for laser and mechanical stimulation.

| Modality | MAE |
|------------|-----------|
| Laser | 0.0102 mm |
| Mechanical | 0.0618 mm |

The lateral inhibition model was further validated using two-point discrimination data from literature. This included two-point discrimination data and gap-detection data. Different stimulation sites were included such as forearm, hand, and finger. The results of the model validation, which is the prediction error calculated by MAE or AE is shown for laser stimulation in Table 4.4 and for mechanical stimulation in Table 4.5. For both

tables the MAE was calculated for the studies above the dashed line and AE calculated for the studies under the dashed line. For the study by Mørch et al. [2010] two-point discrimination data for point-to-point distances between 10 mm and 100 mm was available to be extracted and therefore MAE was calculated. For the rest of the studies only the two-point discrimination threshold was available to be extracted, why the AE was calculated instead.

Table 4.4: Prediction error of the model for laser stimulation. For the studies above the dashed line the MAE was calculated, while AE was calculated for the studies below the dashed line using the two-point discrimination threshold.

| Study | Prediction error | Model output | Threshold | Stimulation area |
|-------------------------|------------------|--------------|-----------|--------------------------------|
| Mørch et al. [2010] | 0.3085 mm | - | - | Forearm |
| Mørch et al. [2010] | 0.3573 mm | - | - | Abdomen |
| Schlereth et al. [2001] | 63.47 mm | 70.17 mm | 6.7 mm | Hand dorsum Radial-ulnar |
| Schlereth et al. [2001] | 59.07 mm | 70.17 mm | 11.1 mm | Hand dorsum Proximal-distal |

Table 4.5: Prediction error of the model for mechanical stimulation. For the studies above the dashed line the MAE was calculated, while AE was calculated for the studies below the dashed line using the two-point discrimination threshold.

| Study | Prediction error | Model output | Threshold | Stimulation area |
|-----------------------------------|------------------|--------------|-----------|--------------------------------|
| Mørch et al. [2010] | 0.0841 mm | - | - | Forearm |
| Mørch et al. [2010] | 0.1455 mm | - | - | Abdomen |
| Schlereth et al. [2001] | 5.03 mm | 12.83 mm | 7.8 mm | Hand dorsum Radial-ulnar |
| Schlereth et al. [2001] | 2.43 mm | 12.83 mm | 10.4 mm | Hand dorsum Proximal-distal |
| Lévêque et al. [2000] | 11.94 mm | 35.24 mm | 23.3 mm | Left forearm |
| Lévêque et al. [2000] | 10.94 mm | 35.24 mm | 24.3 mm | Right forearm |
| Johnson and Phillips [1981] | 11.96 mm | 12.83 mm | 0.87 mm | Finger |
| Martikainen and Pertovaara [2002] | 18.1 mm | 35.4 mm | 17.3 mm | Forearm |

Discussion 5

The purpose of this thesis was to investigate the effect of lateral inhibition on the discriminatory differences between noxious and innocuous stimuli, by designing and implementing artificial neural network (ANN) models. Lateral inhibition is known to be present in the sensory pathways of both noxious and innocuous stimuli with an uncertainty of the mechanisms impact on the spatial discrimination. Using ANN to model lateral inhibition is a method to gain insight on how lateral inhibition impacts spatial discrimination for both modalities. The following is a discussion of the performance of the developed lateral inhibition model and the impact of lateral inhibition on spatial discrimination for noxious and innocuous stimuli. This is elaborated by discussing the process developing, training, and validating the model, and the results obtained from analyzing the model output and testing the predictive accuracy of the model.

An ANN model was developed and trained in MATLAB R2017b (MathWorks inc.) to model lateral inhibition for both noxious and innocuous stimuli. For noxious stimuli the model was trained using data for laser stimulation, while that of innocuous stimuli was trained using mechanical pressure stimulation. The input parameter determining which modality the lateral inhibition model was modelling was the receptive field diameter of either nociceptors or tactile mechanoreceptors. It was shown that the lateral inhibition model for laser stimulation performed better than the lateral inhibition model for mechanical stimulation, when estimating the probability of perceiving one or two points for a given point-to-point distance, based on its similarity to the training data collected from the study by Frahm et al. [2017].

The lateral inhibition model for laser stimulation was overfitted to the training data based on the low prediction error of the model. The performance of the trained model therefore showed to be acceptable in sense that it managed to model the experimental data from Frahm et al. [2017]. A Bland-Altman plot comparing the responses to two-point discrimination acquired with the lateral inhibition model and experimental procedure used as training data showed that the model output generally estimated the training data with a difference between the methods in a interval between -0.02 and 0.03. Around a probability of 0.1 and 0.4 the Bland-Altman plot showed outliers, however these were considered negligible due to the narrow limits of agreement. The narrow limits of agreement indicate that the lateral inhibition model for laser stimulation is overfitted.

The lateral inhibition model for mechanical stimulation showed a two-point discrimination threshold similar to the training data. The corresponding Bland-Altman plot showed that the model output was almost identical to the training data, especially in the probability range of 0.9 and 1. Around a probability of 0.2 and 0.6 the Bland-Altman plot showed

outliers, however these were considered negligible due to the narrow limits of agreement for mechanical stimulation. The upper limits of agreement in the Bland-Altman plot for mechanical stimulation was approximately 5 times the upper limits of agreement for the laser stimulation. This means that the lateral inhibition model for mechanical stimulation estimates the training data with less accuracy at each point-to-point distance. In general the lateral inhibition model for mechanical stimulation estimates with a larger difference compared to the lateral inhibition model for laser stimulation. This is also reflected by the predictive performance of the lateral inhibition model for both modalities, where the lateral inhibition model for laser stimulation showed a better prediction accuracy than the lateral inhibition model for mechanical stimulation. A prediction error for laser stimulation was 0.0102, which for mechanical stimulation was 0.0618. The larger limits of agreement and prediction error showed that the lateral inhibition model for mechanical stimulation was not as fitted to the training data as the lateral inhibition model for laser stimulation. The lateral inhibition for mechanical stimulation have a better predictive performance to new data thereby it is able to poorly generalize solutions.

The difference of the perceived number of points by the lateral inhibition model for mechanical stimulation caused a higher prediction error, hence a lower prediction accuracy compared to the lateral inhibition model for laser stimulation. The lateral inhibition model for both modalities performed with the lowest prediction error on two-point discrimination data from the study by Mørch et al. [2010] compared to the other studies. An explanation may be that the method to collect the two-point discrimination data was most comparable to the training data used during model training. Moreover the data from Mørch et al. [2010] was fitted to a sigmoid just as the training data, and therefore giving a total of 91 prediction errors to calculate a mean from. If the majority of the prediction errors are small then the mean would lean toward being small. This means that the prediction error could be different if only the two-point discrimination threshold was used. It should also be noticed that the experimental design in Frahm et al. [2017] and Mørch et al. [2010] were similar, which may also contribute to the lower prediction error.

For laser stimulation the prediction error of the model in the two-point discrimination threshold for Schlereth et al. [2001] was 59.07 and 63.47, which is further indicative of the lateral inhibition model for laser stimulation being overfitted as the prediction error was high when new data was presented to the model. This is expected by overfitted models since their predictive performance to new data is low and therefore poor at generalizing solutions [da Silva et al., 2017]. The high prediction error could also be attributed to stimulation site being on the dorsum of the hand, since the stimulation diameter was similar to that in Frahm et al. [2017]. For mechanical stimulation the model had a predictive error of 2.43 and 5.03 for the two-point discrimination threshold, thereby performing much better than the model for laser stimulation with regard to the same study, especially considering that the diameter of the stimulation was 1.1 mm and the model was trained only with stimulation diameter of 2.5 mm. The study Lévêque et al. [2000] used a stimulation diameter of 5 mm for mechanical stimulation and the forearm as stimulation site similar to Frahm et al. [2017] and Mørch et al. [2010] though the model for mechanical stimulation had a predictive error of 10.94 and 11.94 being indicative of the two-point discrimination threshold alone is insufficient to validate the model. The studies used for model validation had methodological differences with regard to data collection.

The methodological differences were not modelled, why the lateral inhibition model was limited to the method of acquiring two-point discrimination from the study by Frahm et al. [2017].

Sensitivity analysis

The sensitivity analysis for laser stimulation showed the lateral inhibition model for laser stimulation was sensitive to changes in the receptive field diameter of nociceptors, though decreasing the receptive field diameter to 4.5 mm affected the model output considerably in a negative direction. An increase of the receptive field diameter to 5.5 mm resulted in slight overestimation compared to both training data and the the output of the model for a receptive field diameter of 5 mm. Moreover, the model was very sensitive to stimulation shift regardless of receptive field diameter. It was expected that shifting the stimulation would have an impact, however it was not expected that stimulation shift would result in the response of the model to deviate completely from the training data. The results of the sensitivity analysis for the lateral inhibition model for laser stimulation are further indicative of the model being overfitted, which is especially apparent when considering a receptive field diameter of 4.5 mm, which activates two neurons in the input layer of the model. For a receptive field of 5.5 mm the model only activates one neuron as is the case for a receptive field diameter of 5 mm, which would explain why the model output does not deviate to the same extent.

With regard to the model for mechanical stimulation the sensitivity analysis showed that model was sensitive to changes in the receptive field diameter where a decrease to 2 mm would improve the performance of the model at point-to-point distances 10 mm and 20 mm, which was unexpected considering that training of the model was performed using a receptive field diameter of 2.5 mm. It was expected that the model output would remain similar however with slight differences compared to 2.5 mm. Increasing the receptive field diameter decreased the performance of the model compared to both the 2.5 mm and the training data. Thereby the model was very sensitive to increases of the receptive field diameter. The model was also sensitive to stimulation shift, however this was mainly at point-to-point distances of 10 mm and 20 mm where stimulation shift would improve model performance at for all three receptive field diameters, making them more similar to the training data in that sense.

The results of the sensitivity analysis for the lateral inhibition model for mechanical stimulation show that the model was able to generalize solutions. This was based on all receptive field diameter with and without shift not deviating from the trained model using a receptive field diameter of 2.5 mm, which was not the case for laser stimulation. Decreasing the receptive field diameter to 2 mm lead to the model being fitted better to the training data. Thereby a combination of excitatory and inhibitory field size along with receptive field diameter could be of interest with regard to optimizing the model and possibly achieve a better fitted model.

The model design assumed even spacing between receptive fields with no overlap whatsoever for the purpose of simplifying the model, though it is well-known that overlap in the receptive fields does exists [Kandel et al., 2013]. The degree of overlap is uncertain,

but it would have been of interest to include overlap in the sensitivity analysis.

Model training

The lateral inhibition model was successfully trained with the Gradient descent method using two-points discrimination data from the study by Frahm et al. [2017] as training data. The training resulted in a set of excitatory and inhibitory weights. An analysis of the excitatory weight vector and inhibitory weight vector of 10 seeds showed that the excitatory weight vectors for both modalities were symmetrically decaying from stimulation center, while the inhibitory weight vectors were symmetrically rising from the stimulation center. It has been stated in literature that spatial discrimination of noxious stimulus is lower than for innocuous stimulus [Koltzenburg et al., 1993; Mancini et al., 2014]. This could be attributed to the excitation being more dominant and inhibition less prominent for noxious stimuli. The excitatory field for mechanical stimulation showed to be more protruding than for the laser stimulation, and the inhibitory field for mechanical stimulation being wider than for laser stimulation. Thereby the effect of the lateral inhibition model for mechanical stimulation would result in a better spatial discrimination, which is consistent with literature [Koltzenburg et al., 1993; Mancini et al., 2014]. Both the excitatory and inhibitory weight vectors approached a biological reality by having the characteristics of a Mexican-hat, which is the form attributed to the summation of the excitatory and inhibitory weights, and the spatial distribution after lateral inhibition. The Mexican-hat function for both modalities looked like the excitatory weight vector just bigger in the extremities of the distance caused by the inhibitory field being bigger than the excitatory field. The extremities of the distances looks like having a connection strength equal to 0, but actually it is showing a weak negative connection strength due to the inhibitory field being not big enough compared to the excitatory field and symmetrically rising from the stimulus center. Having a bigger inhibitory field may result in a Mexican-hat function with clear inhibition at the extremities of the distance. The majority of the 10 seeds of excitatory and inhibitory weight vectors for both modalities showed to have a peak at the stimulation center rather than a soft curve. An explanation could be that the updating of the weights stopped too early because of the stop criteria being met, and therefore the weight vector not being entirely smoothed out. This was reflected by the response of the total SSE of the 10 seeds which showed maximum number of iterations performed for updating weight vectors. For laser stimulation 46 iterations were performed, while for mechanical stimulation the number of iterations were 58. The iteration numbers are low for a predictive model and that is due to the constrains implemented during the weight update to keep the weight vectors symmetrically decaying or rising. The weight update without the constrains may have caused the value of some weights to be altered more than others, and in worst case lead to fluctuating weights instead of symmetrical rising or decaying weights. Fluctuating weights were not desired since that would make the lateral inhibition model biological incorrect. The chosen constrains during weight update may have altered the learning rate, why the iteration number was low and rise and decay of the weight vectors not more gradually changing. Implementing the constrains made the training with the Gradient descent method deviate from its intended purpose of reducing the SSE for each weight in the weight vectors. The weight would be updated to achieve a lower SSE, where the constrain may have impacted the weight update by reversing it

resulting in a higher SSE. The model training ignored this fact and accounted for total SSE, when determining to stop the model training. This may explain why some weights were more altered after training than others. It was also noticeable that the size of the excitatory and inhibitory weight vector impacted on the model training. The size of the excitatory weight vector was determined by R_1 and inhibitory weight vector by R_2 . It is known from physiology that inhibitory field is wider than the excitatory field. Both R_1 and R_2 were altered to a new set of R_1 and R_2 using an algorithm, which would result in the lowest prediction error after training. The initial optimal R_1 and R_2 were increased using the constraints of $R_2 > R_1$ and the maximum value of R_1 and R_2 to be 30. The algorithm resulted in identical set of R_1 and R_2 for both modalities, which is not an issue, since there is no evidence pertaining to the ratio between excitatory and inhibitory fields or whether this ratio would be different depending on modality. Altering R_1 and R_2 resulted in the lateral inhibition model for laser stimulation to fit the training data, which was desired. However, the lateral inhibition model for mechanical stimulation fitted the training data poorly compared to the lateral inhibition model for laser stimulation.

Ideally a learning algorithm that updates the excitatory and inhibitory weights while keeping them symmetrically rising or decaying without any constraints was desired. The Gradient descent method did not meet the desired learning algorithm, why constraints were implemented. The simplicity of the lateral inhibition model limited the complexity of the learning capabilities for model. The lateral inhibition model was developed as a single-layer ANN, since the excitatory and inhibitory field was combined in the output layer, resulting in no hidden layers making the predictive ability harder to train. An alternative design of the lateral inhibition model could be to separate the excitatory and inhibitory fields as two separate layers in the model developing a multi-layer ANN with two hidden layers. This would increase the complexity of the model and the output layer would not be modelled as the Mexican-hat model which incorporates excitatory and inhibitory lateral connections between the output neurons. The complexity of the multi-layer ANN lies in determining the number of hidden layers as well as the learning parameters e.g. initial weights [Al-Kaf et al., 2018]. It may not be that two hidden layers are right for the model, and determining the correct number of hidden layers may lead to many attempts using the trail-and-error method [Al-Kaf et al., 2018]. The number of hidden neurons is important since overfitting of the model may occur if too many hidden neurons are used [Al-Kaf et al., 2018]. The output of the lateral inhibition model would be the same regardless of the ANN topology, where the one with no hidden layers explicitly implements the lateral connections. The advantage of modelling the lateral inhibition model as a multi-layer ANN is that there are more weights to adjust, which may give a better generalized solution than a single-layer ANN if a correct number of hidden layers is used.

Model Development

The lateral inhibition model was developed with different through different designs and architectures before implementing the final design. In literature lateral inhibition is typically modelled as either a feed-forward network or feedback network [Strominger et al., 2012; R.Collier et al., 1996]. Developing a lateral inhibition model using feedback is typically done with the purpose of investigating contrast enhancement [R.Collier et al.,

1996; Fausett, 1994]. The lateral inhibition model developed during this thesis did not focus on contrast enhancement and it was considered excessive to introduce a feedback loop, why it was chosen not to. The final model was developed as a single layer network to simplify the model, thus excitation and inhibition occurred in the same layer.

Earlier model designs did not involve the implementation of an artificial neural network, but instead a regular network model. The models presented in Appendix E Figure E.1 and Figure E.3 were designed as a partially connected networks, where the input nodes represented 10 mm on the forearm. The weightings were different for laser and mechanical stimulation account for the difference between noxious and innocuous stimuli literature [Koltzenburg et al., 1993; Mancini et al., 2014]. Thus, the input was designed such that the symmetrical decay for would be less prominent for laser stimulation compared to mechanical stimulation.

The output layer of the model in Figure E.1 consisted of 31 neurons which were used to represent the spatial distribution. It was determined that more connections would result in better resolution of the spatial distribution, which was the reasoning for having five connections. The model could not provide the probability of perceiving one or two points, why it was revised. The revised model design in Figure E.3 was based on the conceptual model of lateral inhibition by Kandel et al. [2013], though without feedback connections. Moreover, the second layer represented inhibitory interneurons. The output of this model was the probability of the perceiving one or two points.

Both designs were discarded for several reasons. The input neurons were input layer being represented distance on the forearm, which was too large compared to the stimulation diameter of 5 mm. For the final model the input layer was changed to the receptive field diameter of nociceptors and tactile mechanoreceptors being 5 mm and 2.5 mm respectively. Both designs used manually fixed weightings making them impossible to train. The output of the first model provided the spatial distribution, but not probability of perceiving one or two points, while second model provided the probability of perceiving one or two points, but not the spatial distribution. In general, both designs introduced vast subjectivity, which was not sensible for development of a model which aimed to provide insight on the different effects of a sensory mechanism on discriminatory differences. The output layer of the final model was implemented as a Mexican-hat model introduced by Kohonen [1982] and provided both the spatial distribution along with probability of perceiving one or two points.

Conclusion 6

The purpose of this thesis was to develop an artificial neural network (ANN) to investigate the effect of lateral inhibition on the discriminatory differences between noxious and innocuous stimuli. A single-layer ANN was developed and trained in MATLAB R2017b (MathWorks inc.) modelling lateral inhibition for both noxious and innocuous stimuli. The lateral inhibition model for noxious stimuli was trained using data for laser stimulation, while that of innocuous stimuli was trained using mechanical pressure stimulation. The two-point discrimination data used during model training was acquired from the study by Frahm et al. [2017].

The lateral inhibition model for laser stimulation was able to fit the training data with a prediction error of 0.0102 mm. The model was not able to generalize solutions due to being overfitted and resulting in poor performance when presented with new data, as shown during model validation. The lateral inhibition model for laser stimulation performed with the lowest prediction error being between 0.3085 mm and 0.3573 mm with two-point discrimination data from Mørch et al. [2010]. With two-point discrimination data from other studies the model performed with a prediction error between 59.07 mm and 63.47 mm, confirming that the lateral inhibition model for laser stimulation was overfitted.

The lateral inhibition model for mechanical stimulation was able to fit the training data with prediction accuracy of 0.0618 mm. The lateral inhibition model for mechanical stimulation was not overfitted compared to the lateral inhibition model for laser stimulation, and therefore able to poorly generalize solutions, when presented with new data, as shown during model validation. The lateral inhibition model for mechanical stimulation performed with the lowest prediction error being between 0.0841 mm and 0.1455 mm with two-point discrimination data from Mørch et al. [2010]. The models ability to poorly generalize solutions was reflected by performing with a prediction error between 2.43 mm and 18.1 mm with two-point discrimination data from other studies.

Designing, implementing and validating an ANN that modelled lateral inhibition for both noxious and innocuous stimuli to investigate the discriminatory differences between both modalities was achieved.

Bibliography

- Al-Kaf et al., 2018.** Hasan Ali Gamal Al-Kaf, Kim Seng Chia and Nayef Abdulwahab Mohammed Alduais. *A comparison between single layer and multilayer artificial neural networks in predicting diesel fuel properties using near infrared spectrum*. *Petroleum Science and Technology*, 36(6), 411–418, 2018.
- Altman and Bland, 1999.** D. G. Altman and J. M. Bland. *Measuring agreement in method comparison studies*. *Statistical Methods in Medical Research*, 8(1), 135–160, 1999.
- Altman and Bland, 1983.** D. G. Altman and J. M. Bland. *Measurement in Medicine: The Analysis of Method Comparison Studies*. *Journal of the Royal Statistical Society. Series D (The Statistician)*, 32(3), 307–317, 1983.
- Betts et al., 2017.** J. Gordon Betts, Peter Desaix, Eddie Johnson, Jody E. Johnson, Oksana Korol, Dean Krusea, Brandon Poe, James A. Wise, Mark Womble and Kelly A. Young. *Anatomy & Physiology*. Rice University, 2017.
- Bromm et al., 1984.** B. Bromm, M. T. Jahnke and R. D. Treede. *Responses of Human Cutaneous Afferents to CO₂ Laser Stimuli Causing Pain*. *Experimental Brain Research*, 55(1), 158–166, 1984.
- Chai and Draxler, 2014.** T. Chai and R. R. Draxler. *Root mean square error (RMSE) or mean absolute error (MAE)? – Arguments against avoiding RMSE in the literature*. *Geoscientific Model Development*, 7(1), 1247–1250, 2014.
- da Silva et al., 2017.** Ivan Nunes da Silva, Danilo Hernane Spatti, Rogerio Andrade Flauzino, Luisa Helena Bartocci Liboni and Silas Franco dos Reis Alves. *Artificial Neural Networks: A Practical Course*. Springer International Publishing Switzerland, 1 edition, 2017.
- D’Mello and Dickenson, 2008.** R. D’Mello and A. H. Dickenson. *Spinal cord mechanisms of pain*. *British Journal of Anaesthesia*, 101(1), 8–16, 2008.
- Elizondo and Fiesler, 1997.** D. Elizondo and E. Fiesler. *A survey of partially connected neural networks*. *International Journal of Neural Systems*, 8(5-6), 535–58, 1997.
- Fausett, 1994.** Laurene Fausett. *Fundamentals of Neural Networks: Architectures, algorithms and Applications*. Pearson, 1 edition, 1994.
- Feher, 2017.** Joseph Feher. *Quantitative Human Physiology: An Introduction*. Elsevier, 2 edition, 2017.

- Frahm et al., 2017.** Ken Steffen Frahm, Carsten Dahl Mørch and Ole Kæseler Andersen. *Tempo-spatial discrimination is lower for noxious stimuli than for innocuous stimuli.* The Journal of the International Association for the Study of Pain, 0(0), 1–9, 2017.
- Hardy et al., 1940.** J. D. Hardy, H.G. Wolff and H. Goodell. *A new method for measuring pain threshold: observations on spatial summation of pain.* Journal of Clinical Investigation, 19(4), 649–657, 1940.
- Hennig et al., 2008.** Patrick Hennig, Ralf Möller and Martin Egelhaaf. *Distributed Dendritic Processing Facilitates Object Detection: A Computational Analysis on the Visual System of the Fly.* Plos One, 3(8), 1–14, 2008.
- Hollins et al., 2011.** Mark Hollins, Daniel Harper and William Maixner. *Changes in Pain from a Repetitive Thermal Stimulus: The Roles of Adaptation and Sensitization.* The Journal of the International Association for the Study of Pain, 152(7), 1583–1590, 2011.
- Johnson, 2001.** Kenneth O. Johnson. *The roles and functions of cutaneous mechanoreceptors.* Current Opinion in Neurobiology, 11(4), 455–461, 2001.
- Johnson and Phillips, 1981.** Kenneth O. Johnson and John R. Phillips. *Tactile spatial resolution. I. Two-point discrimination, gap detection, grating resolution, and letter recognition.* Journal of Neurophysiology, 46(6), 1177–1191, 1981.
- Kandel et al., 2013.** Eric R. Kandel, James H. Schwartz, Thomas M. Jessel, Steven A. Siegelbaum and A. J. Hudspeth. *Principles of Neural Science.* The McGraw-Hill Companies Inc., 5 edition, 2013.
- Kohonen, 1982.** Teuvo Kohonen. *Self-Organized Formation of Topologically Correct Feature Maps.* Biological Cybernetics, 43(1), 59–69, 1982.
- Koltzenburg et al., 1993.** Martin Koltzenburg, Hermann O. Handwerker and H. Erik Torebjörk. *The ability of humans to localise noxious stimuli.* Neuroscience Letters, 150, 219–222, 1993.
- Lévêque et al., 2000.** Jean-Luc Lévêque, Johanna Dresler, Edith Ribot-Ciscar, Jean-Pierre Roll and Christine Poelman. *Changes in Tactile Spatial Discrimination and Cutaneous Coding Properties by Skin Hydration in the Elderly.* The Society for Investigative Dermatology, 115(3), 454–458, 2000.
- Mancini et al., 2014.** F. Mancini, A. Bauleo, J. Cole, F. Lui, C.A. Porro, P. Haggard and G. D. Iannetti. *Whole-body mapping of spatial acuity for pain and touch.* Annals of Neurology, 75(6), 917–24, 2014.
- Martikainen and Pertovaara, 2002.** Ilkka K. Martikainen and Antti Pertovaara. *Spatial discrimination of one versus two test stimuli in the human skin: dissociation of mechanisms depending on the task and the modality of stimulation.* Neuroscience Letters, 328(3), 322–324, 2002.
- Martini et al., 2015.** Frederic H. Martini, Judi L. Nath and Edwin F. Bartholemew. *Fundamentals of Anatomy and Physiology.* Pearson, 10 edition, 2015.

- McCulloch and Pitts, 1943.** Warren McCulloch and Walter Pitts. *A logical calculus of the ideas immanent in nervous activity*. The bulletin of mathematical biophysics, 5 (4), 115–133, 1943.
- McGee, 2018.** Steven McGee. *Evidence-based physical diagnosis*. Elsevier, 4 edition, 2018.
- Mørch et al., 2010.** C. D. Mørch, O. K. Andersen, A. S. Quevedo, L. Arendt-Nielsen and R. c. Coghill. *Exteroceptive aspects of nociception: insights from graphesthesia and two-point discrimination*. The Journal of the International Association for the Study of Pain, 151(1), 45–52, 2010.
- Negnevitsky, 2005.** Michael Negnevitsky. *Artificial Intelligence: A Guide to Intelligent Systems*. Pearson, 2 edition, 2005.
- Premkumar, 2004.** Kalyani Premkumar. *The Massage Connection: Anatomy and Physiology*. Lippincot Williams & Wilkins, 2 edition, 2004.
- Price et al., 1989.** Donald D. Price, John G. McHaffie and Michelle A. Larson. *Spatial Summation of Heat-Induced Pain: Influence of Stimulus Area and Spatial Separation of Stimuli on Perceived Pain Sensation and Unpleasantness*. Journal of Neurophysiology, 62(6), 1270–1279, 1989.
- Quevedo et al., 2017.** Alexandre S. Quevedo, Carsten Dahl Mørch, Ole Kæseler Andersen and Robert C. Coghill. *Lateral inhibition during nociceptive processing*. The Journal of the International Association for the Study of Pain, 158, 1046–1052, 2017.
- R.Collier et al., 1996.** Joanne R.Collier, Nicholas A.M.Monk, Philip K. Maini and Julian H. Lewis. *Pattern Formation by Lateral Inhibition with Feedback: a Mathematical Model of Delta-Notch Intercellular Signalling*. Journal of Theoretical Biology, 183(4), 429–446, 1996.
- Rosenblatt, 1958.** F. Rosenblatt. *The perceptron: A probabilistic model for information storage and organization in the brain*. Psychological Review, 65(6), 386–408, 1958.
- Sazli, 2006.** Murat Hüsnü Sazli. *A brief review of feed-forward neural networks*. Communications, Faculty Of Science, University of Ankara, 50, 11–17, 2006.
- Schlereth et al., 2001.** T. Schlereth, W. Magerl and R. Treede. *Spatial discrimination thresholds for pain and touch in human hairy skin*. The Journal of the International Association for the Study of Pain, 92(1-2), 187–194, 2001.
- J. Sirosh and R. Miikkulainen, march-april 1993.* J. Sirosh and R. Miikkulainen. How Lateral Interaction Develops in a Self-Organizing Feature Map. In *IEEE International Conference on Neural Networks (San Fransisco, CA)*. IEEE, march-april 1993.
- Strominger et al., 2012.** Norman L. Strominger, Robert J. Demarest and Lois B. Laemle. *Noback's Human Nervous System: Structure and Function*. Springer Science, 7 edition, 2012.
- Treede et al., 2003.** Rolf-Detlef Treede, Jürgen Lorenz and Ulf Baumgärtner. *Clinical usefulness of laser-evoked potentials*. Clinical Neurophysiology, 33(6), 303–314, 2003.

Wallach and Goffinet, 1989. D. Wallach and B. Goffinet. *Mean Squared Error of Prediction as a Criterion for evaluating and Comparing System Model.* Ecological Modelling, 44(1), 299–306, 1989.

Sensory pathways A

Noxious stimuli are conveyed through the spinothalamic tract, while innocuous stimuli are conveyed through the dorsal column pathway. [D'Mello and Dickenson, 2008] Both pathways are illustrated in Figure A.1.

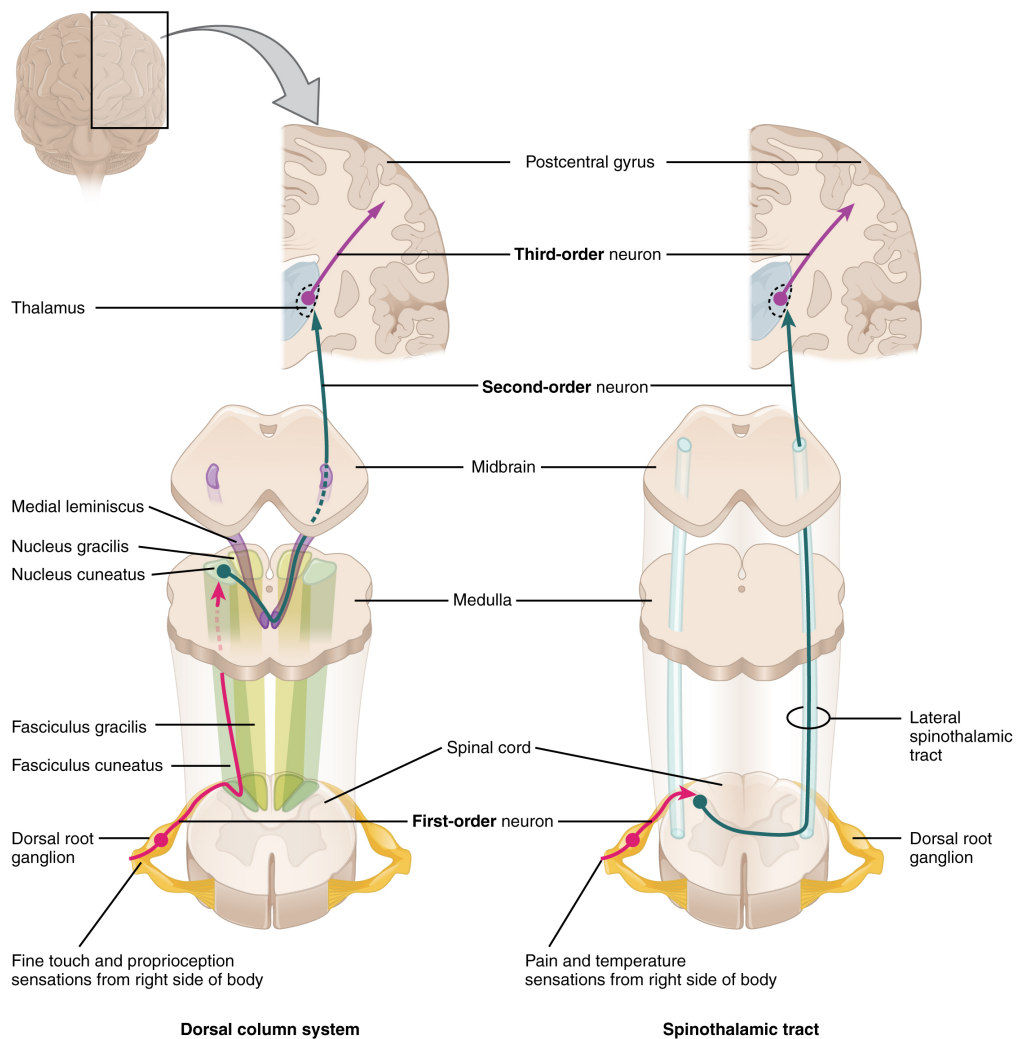


Figure A.1: Both innocuous stimuli and noxious stimuli ascend to the thalamus but through different pathways. The dorsal column pathway conveys innocuous stimuli and the spinothalamic tract conveys noxious stimuli. [Betts et al., 2017]

During stimulation of the high-threshold A- δ fibers and C fibers the afferent signal

terminates on interneurons located in the dorsal root of the spinal cord where the information is processed. Noxious information is mainly processed in nociceptive specific cells, which are located in the superficial layers laminae I and laminae II [D'Mello and Dickenson, 2008]. The noxious information is bifurcated and ascend through the anterolateral tract and the lateral spinothalamic tract that is comprised of second order neurons responsible for further processing in the thalamus. [Strominger et al., 2012; Feher, 2017]

Stimulation of A- β fibers leads to the afferent signal being conveyed through the dorsal column pathway. The afferent signal terminates in the spinal dorsal horn where it is processed in laminae III-V [D'Mello and Dickenson, 2008]. The afferent information is conveyed toward the nucleus cuneatus and medulla through the spinal tracts fasciculus cuneatus and the fasciculus gracilis which is comprised of second order neurons. [Strominger et al., 2012; Feher, 2017]

It has been established that noxious and innocuous stimuli are conveyed through different pathways. It is possible to modulate noxious stimuli with innocuous mechanical stimuli in the spinal dorsal horn based on the gate control theory. [Strominger et al., 2012] Figure A.2 illustrates the concept of gate control theory.

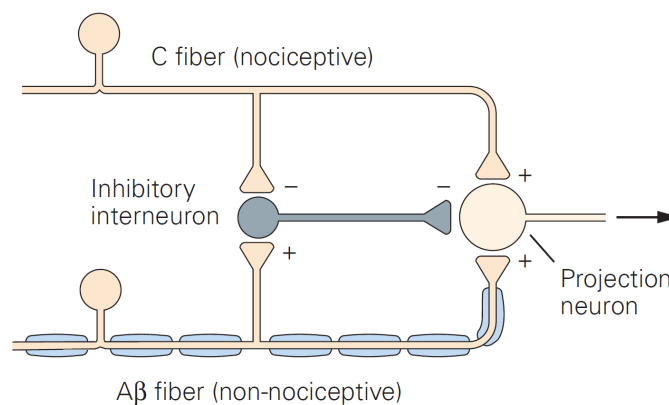


Figure A.2: Concept of the gate control theory which shows the pathway of nociceptive and non-nociceptive stimuli through the projection neuron. Nociceptive stimuli inhibits the inhibitory interneuron opening the gate allowing projection to the Thalamus. Non-nociceptive stimuli activates the inhibitory interneuron, closing the gate preventing projection to the Thalamus. [Betts et al., 2017; Kandel et al., 2013]

Stimulation of non-nociceptive fibers cause excitation of the inhibitory interneuron and the projection neuron, however activation of the inhibitory interneuron closes the gate which in turn prevents the information from reaching the thalamus. Stimulation of a nociceptor prevents excitation of the inhibitory interneuron which allows the gate to open. Thereby the projection neuron will be able to transmit the signal to the Thalamus. During activation of nociceptors the gate control theory normally allows for the projection neuron to transmit the information to the Thalamus, thereby ensuing an increased perception of pain. However when simultaneously activating the non-nociceptive fibers the pain is modulated by the non-nociceptive fibers, as the inhibitory interneuron becomes active, thus altering the behavior of the projection neuron. [Strominger et al., 2012]

Experimental procedure

B

The subjects were comfortably seated on a bed with the backrest inclined, and their right forearm positioned horizontally during both mechanical and laser stimulation. The subjects were prior to the stimulation prepared by shaving excessive hair growth in the area of stimulation. The order of the stimulus modality was randomized between subjects.

The spatial acuity during both stimulation modalities was evaluated using the two-point discrimination threshold, which tests the ability of the subjects to distinguish two points of stimulation simultaneously applied to the skin. The test was conducted by applying single and two-point stimulations, using a forced choice design, subjects were to indicate whether they perceived one or two points as well as indicate the intensity after each stimulation. The intensity for laser stimulation was specified with a numeric rating scale (NRS), where 0 was the perception threshold, 3 the pain threshold, and 10 as maximum pain perceived. The same NRS was used for mechanical stimulations. Since the intensity thereof was not painful it was expected to be perceived below the pain threshold. When stimulating two points, a point-to-point distance between 10 and 100 mm, in steps of 10 mm were used. Each step is a trial and was applied twice in a randomized order giving in total 20 trials per stimulation modality.

Laser stimulation

The laser stimulation was applied by a Synrad Firestar ti-series 100 W CO₂ laser (Synrad, Mukilteo, WA) to deliver noxious heat stimuli on the skin. The two-point stimulation was delivered from point-to-point by the laser. Protective goggles were worn during the experiment. In order to project the laser beam, a scanner head (GSI Lumonics; General Scanning XY10A) was used, which consists of two galvanometers with mounted mirrors. The scanner head projected a laser beam on one spot or alternating between two spots in a quick and accurate manner, providing a stimulation to either be perceived as one or two points lasting for 1.5 seconds. Each laser beam had a diameter of 5 mm ($1/e^2$), which was achieved by dithering the laser beam; quickly displacing the laser beam in small concentric circles. Dithering did not impact on how the stimulations were perceived. The intensity delivered by the laser was adjusted such that the subject perceived a laser beam as 4 on the NRS, slightly above the pain threshold. The interstimulus interval was between 30 and 60 seconds in order to avoid habituation and sensitization due to cumulative effect of heat during repeated stimulations [Hollins et al., 2011; Treede et al., 2003; Quevedo et al., 2017]. An infrared camera (Agema 900 series) was used to monitor the skin temperature was during repetitive laser stimulations. For the safety of the subject, the experiment was discontinued if the temperature of the skin surpassed 60°C to avoid tissue damage due noxious stimuli [Kandel et al., 2013]. The infrared camera was also used to ensured a

Gaussian-like profile for the laser beam.

Mechanical stimulation

The mechanical stimulation was applied as touch by two blunt plastic filaments mounted to a Vernier caliper. The plastic filaments have a diameter of 5mm, and the same Vernier caliper was used to stimulate one or two points. The stimulations was applied with great precision to ensure both filaments simultaneously touched the skin during two-points stimulation.

Self-organizing neural networks



Self-organizing neural networks are completely connected single layer networks and have their foundation in competitive learning, which is presented in the following.

In competitive learning the neurons compete amongst themselves to become activated and only a single output neuron can be active at a time, compared to Hebbian learning where several output neurons can be active at a time. Competitive learning relies on a winner-takes-all approach. Self-organizing maps referred to as Kohonen networks was introduced by Kohonen [1982], which are based on competitive learning. The general architecture of a Kohonen network is illustrated in Figure C.1. [Negnevitsky, 2005]

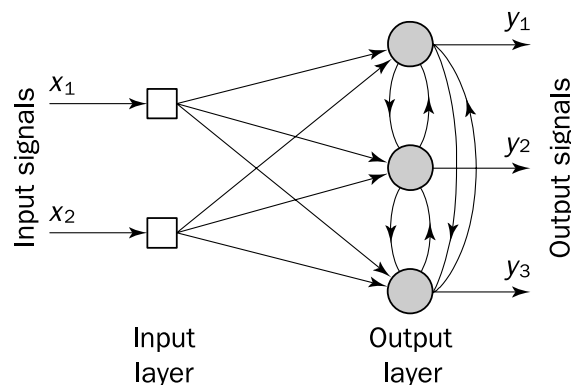


Figure C.1: General architecture for the Kohonen network. [Negnevitsky, 2005]

The Kohonen network is composed by a single layer of computational neurons, but with two different types of connections (1) forward connections from the input neurons to the output neurons, and (2) lateral connections between the output neurons. The function of the lateral connections is to create a competition between neurons in the output layer. The neuron with the highest level of activation in the output layer becomes the winning neuron and he only one to produce and any output signal while the activity of the other neurons will be suppressed. When the Kohonen network receives an input pattern, each of the Kohonen layer neurons get the same copy of the input pattern, however it becomes modified through the synaptic weights of the connections between the input layer and Kohonen layer. The lateral connection produce either excitatory or inhibitory effects which is dependent on the distance from the winning neuron. The synaptic weights between neurons in the Kohonen layer can be described by the Mexican hat function illustrated in Figure C.2. [Negnevitsky, 2005]

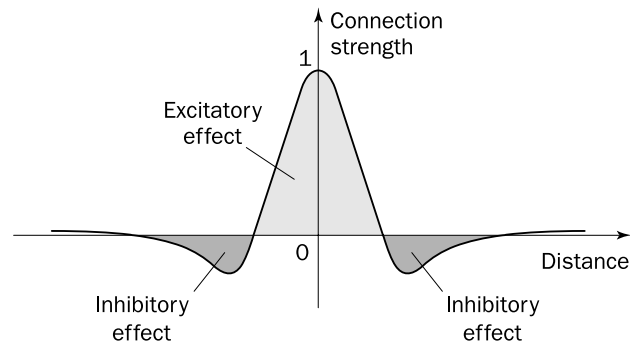


Figure C.2: Illustration of the Mexican hat function of lateral inhibition, which is comprised of excitatory effect in the middle and inhibitory effect on both lateral sides. [Negnevitsky, 2005]

The figure demonstrates the relationship between distance from the winning neuron and the strength of connections in the Kohonen layer. The close-range neighborhood has a strong excitatory effect while the midrange neighborhood has a mild inhibitory effect, and long-range neighborhood has a strong inhibitory effect. In the Kohonen network only winning neuron and its neighborhood are able to learn. The winning neuron j has its output y_j set equal to one and the output signal of the losing neurons are set equal to zero. The standard competitive learning rule is defined by Equation C.1 [Negnevitsky, 2005]

$$\Delta w_{ij} = \begin{cases} \alpha(x_i - w_{ij}), & \text{if neuron } j \text{ wins the competition} \\ 0, & \text{if neuron } j \text{ loses the competition} \end{cases} \quad (\text{C.1})$$

Where Δw_{ij} is the change applied to the synaptic weights w_{ij} . The input is given by x_i and the learning parameter by α which has a value between 0 and 1. The key feature of the competitive learning rule is moving the synaptic weight vector \mathbf{W}_j of the winning neuron j toward the input \mathbf{X} . The criterion used to determine the winning neuron is the Euclidian distance d which is defined by Equation (C.2), where x_i is the i th element of \mathbf{X} and w_j of \mathbf{W} . [Negnevitsky, 2005]

$$d = \|\mathbf{X} - \mathbf{W}\| = \left[\sum_{i=1}^n (x_i - w_{ij})^2 \right]^{\frac{1}{2}} \quad (\text{C.2})$$

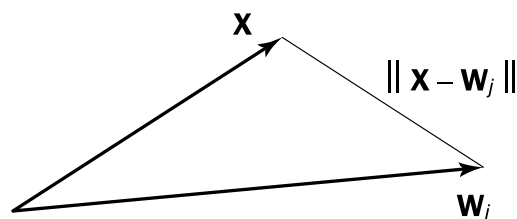


Figure C.3: Illustration of how Euclidian distance can be used as a similarity measure between vector \mathbf{X} and \mathbf{W}_j [Negnevitsky, 2005]

The smaller the Euclidian distance the greater the similarity is between \mathbf{X} and \mathbf{W} . Thus, in order to determine the winning neuron $j_{\mathbf{X}}$ that is most similar to input \mathbf{X} the smallest Euclidian distance is used as shown in Equation (C.3) [Negnevitsky, 2005]

$$j_{\mathbf{X}} = \min_j \|\mathbf{X}_j - \mathbf{W}_j\| \quad j = 1, 2, \dots, m \quad (\text{C.3})$$

Where m is the number of outputs in the Kohonen layer. Based on the previous the competitive learning algorithm is derived. The first is initialization. During this step the initial synaptic weights and threshold are assigned random values between 0 and 1. Learning rate α is assigned a positive value. The Kohonen network is activated by applying the input vector \mathbf{X} and detmining the winning neuron $j_{\mathbf{X}}$ using the minimum Euclidian distance at iteraton p as shown in Equation (C.4). [Negnevitsky, 2005]

$$j_{\mathbf{X}}(p) = \min_j \|\mathbf{X} - \mathbf{W}_j(p)\| = \left\{ \sum_{i=1}^n [x_i - w_{ij}(p)]^2 \right\}^{\frac{1}{2}} \quad (\text{C.4})$$

where n is the number of input neurons, and m is the number of neurons in the Kohonen layer. The following step is updating of synaptic weights:

$$w_{ij}(p+1) = w_{ij}(p) + \Delta w_{ij}(p) \quad (\text{C.5})$$

where $\Delta w_{ij}(p)$ is the weight correction at iteration p . The update of synaptic weights is determined by the competitive learning rule

$$\Delta w_{ij} = \left\{ \begin{array}{ll} \alpha[x_i - w_{ij}], & j \in \Lambda_j(p) \\ 0, & j \notin \Lambda_j(p) \end{array} \right\} \quad (\text{C.6})$$

where α is the learning parameter, and $\Lambda_j(p)$ is the neighborhood function centered around the winning neuron $j_{\mathbf{X}}$ at iteration p . $\Lambda_j(p)$ has a constant amplitude and implies simultaneous activation of all neurons located within the neighborhood as illustrated on Figure C.4. [Negnevitsky, 2005]

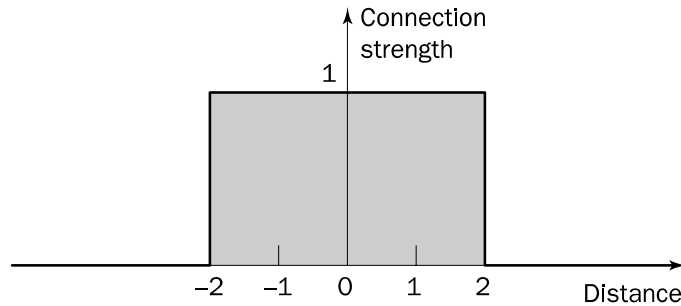


Figure C.4: Illustration of the rectangular neighborhood function. [Negnevitsky, 2005]

The relationship between those neurons is independent from the distance to $j_{\mathbf{X}}$. It has a binary form as shown in Equation (C.7)

$$y_j = \begin{cases} 1, & j \in \Lambda_j(p) \\ 0, & j \notin \Lambda_j(p) \end{cases} \quad (\text{C.7})$$

Iteration p is increased and steps 2 to 4 are repeated until the Euclidean distance criterion is satisfied.

Results for lateral inhibition model for laser stimulation

D

The lateral inhibition model for laser stimulation with the initial optimal radius for the excitatory region $R_1 = 6$ and inhibitory region $R_2 = 10$. The model generally performed poorly due to the small used. Due to the choice of R_1 and R_2 training of the model resulted in a poorly performing model. This is reflected by the total SSE during model training shown in Figure D.1. The response of the total SSE per iteration for 10 seeds calculated during model training is shown in Figure D.1. The total SSE for laser stimulation show a decline for all seeds, however some seeds do not reach a minimum total SSE before training is ended resulting in a poorly performing model.

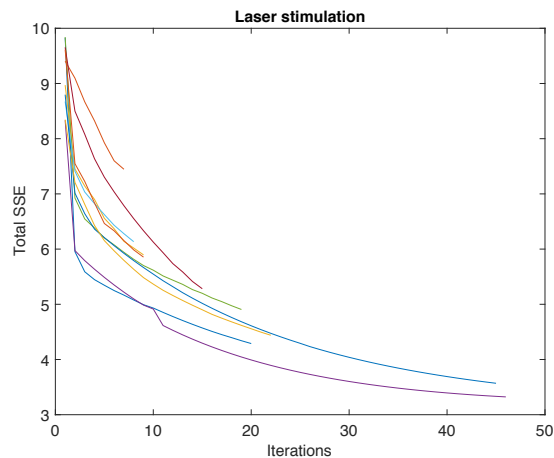


Figure D.1: Response of the total SSE of 10 seeds for laser stimulation as the number iterations increase.

To analyze the characteristics of the excitatory and inhibitory weights with regard to biological reality the weights vectors were extracted for 10 seeds, after model training. Moreover, the summation of the weight vectors were plotted to determine if they had they had Mexican-hat shape. The weights summation thereof are shown in Figure D.2, for laser stimulation. The excitatory weights for both modalities showed symmetrical decay from stimulation center, while the inhibitory weights show symmetrical rise from the stimulation center. The summated weights show a Mexican hat shape.

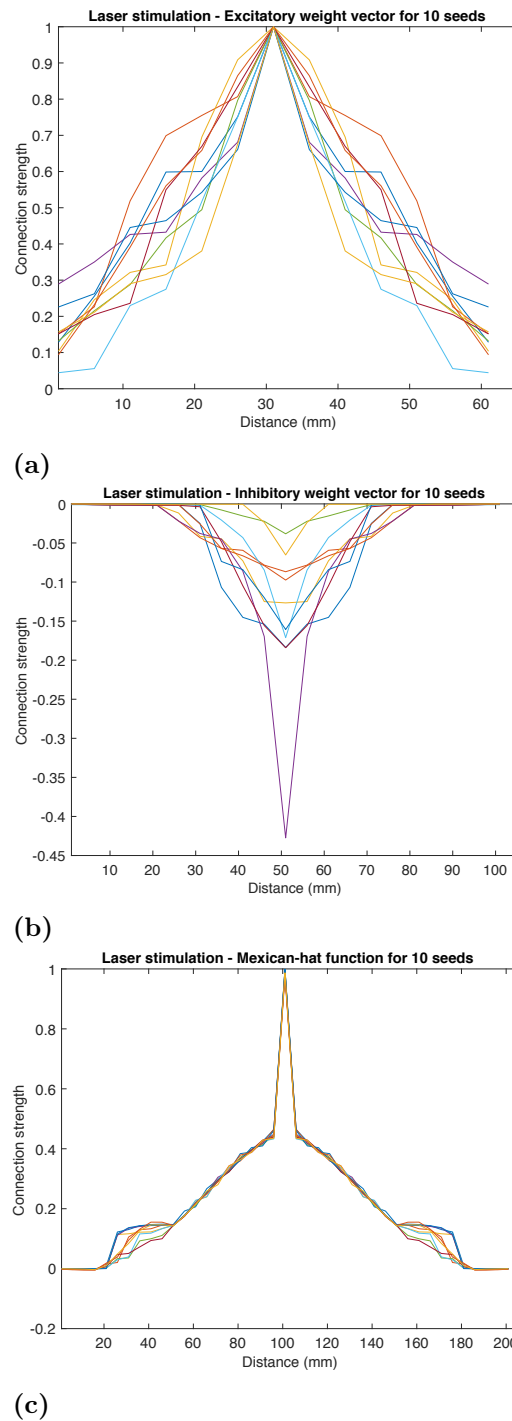


Figure D.2: The weight vectors of 10 seeds, after model training for laser stimulation. The excitatory weights are shown in (a) while the inhibitory weights are shown in (b). The summated of the excitatory and inhibitory weights are shown in (c). The summations show a Mexican-hat like shape.

To analyze the response to two-point discrimination for laser stimulation, the responses to the two-point discrimination for trained lateral inhibition model were plotted for 10 seeds at point-to-point distances from 10 mm and 100 mm, and are shown in Figure D.3. Moreover the sigmoidal curve fitted from the training data which indicated by a thick blue line was plotted. The point where the dashed line intersects with the curves are the

two-point discrimination threshold.

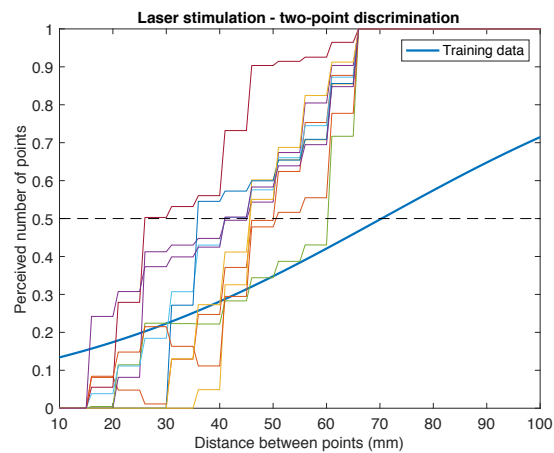


Figure D.3: Probability of perceiving one or two points when changing the point-to-point distance between stimulations for laser stimulation stimulation. Each plot shows 10 seeds per modality. The training data is shown in thick blue line and the dashed line indicates the 50 % threshold of perceiving one of two points.

To analyze the agreement between model output and find where the model differs from the training data a Bland-Altman plot comparing the model output and training data for laser stimulation. The Bland-Altman plots are shown in Figure D.4. The parameters of the Bland-Altman plot are in Table D.1. The model had a tendency to overestimate the probability of perceiving one or two points compared to the training data, as seen from the mean bias of 0.22. The model showed no outliers and when introducing a new measurement to the model, the output would with a 95 % certainty lie within the limits of agreement. Notice that the upper limit of agreement is at 0.69, since the mean number of perceived number of points from approximately 0.7 and after are overestimated. The model underestimates the mean perceived number of points according to the training data, when the probability of the stimulations being perceived as two points is under 0.2. From the two-point discrimination threshold the model overestimates the probability of stimulations being perceived as one or two points. Therefore, the model output approaches the training data best with the least under- and overestimation between the mean perceived number of points of approximately 0.2 and 0.3.

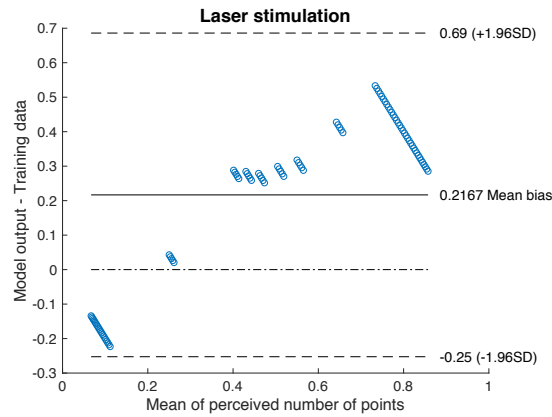


Figure D.4: The Bland-Altman plot of the comparison between the model output and the training data for laser stimulation. Each dot corresponds to the difference between the output of the lateral inhibition model and the training data as the probability of a stimulation to be perceived as two points. The Bland-Altman is presented a total of 91 points, one for each point-to-point distance from 10 mm to 100 mm with a step of 1 mm. The x-axis show mean perceived number of points, where 0 corresponds to one point and 1 corresponds to two points.

Table D.1: The parameters used to calculate the confidence interval for the Bland-Altman plot of each modality.

| Parameter | Laser stimulation |
|-----------------------------------|--------------------|
| Mean bias | 0.2167 |
| Standard deviation of differences | 0.0215 |
| 95% Limits of agreement | from -0.25 to 0.69 |

Previous model designs

E

The following contains previous network designs, which were initially considered to model lateral inhibition. The process behind the overall design and the different layers of the networks are explained, along with why these designs were eventually discarded.

Model design 1

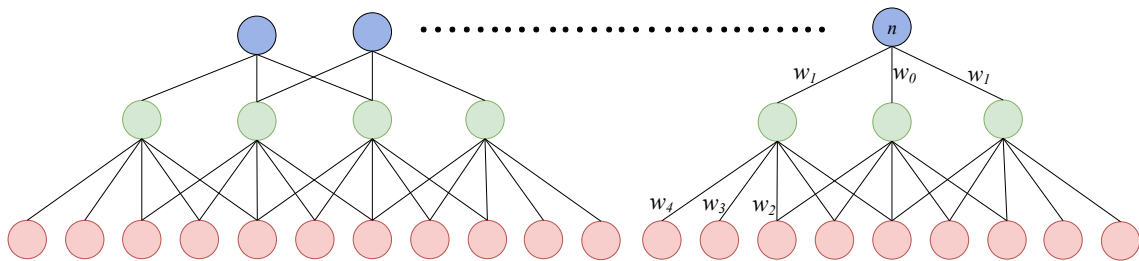


Figure E.1: The first design of the lateral inhibition model.

The design in Figure E.1 shows a partially connected neural network with intended 12 nodes in the input layer, where each node represents 10 mm on the forearm, and the two outer neurons are required so that the stimuli can be modelled properly without cutting the delivered input. The input delivered in the first layer diverges to three adjacent neurons in the following layer. The values of the weights w_0 and w_1 were chosen in order to achieve symmetrical decay from the stimulus center. The values themselves would be different for mechanical stimulation and laser stimulation to model the difference between noxious and innocuous stimuli, thus the decay for mechanical stimulation would be more prominent, than for the laser stimulation.

The output layer consists of 31 neurons which are used to represent the achieved spatial distribution of the stimuli on the forearm and would be used to determine whether one or two-points were perceived during stimulation. Each node in the second layer has five connections to the output layer. It was determined that more connections would result in better resolution of the spatial distribution, which was the reasoning behind having five connections. The weights $w_2 > w_3 > w_4 < 0$ where chosen to achieve lateral inhibition in the stimulation.

Model design 2

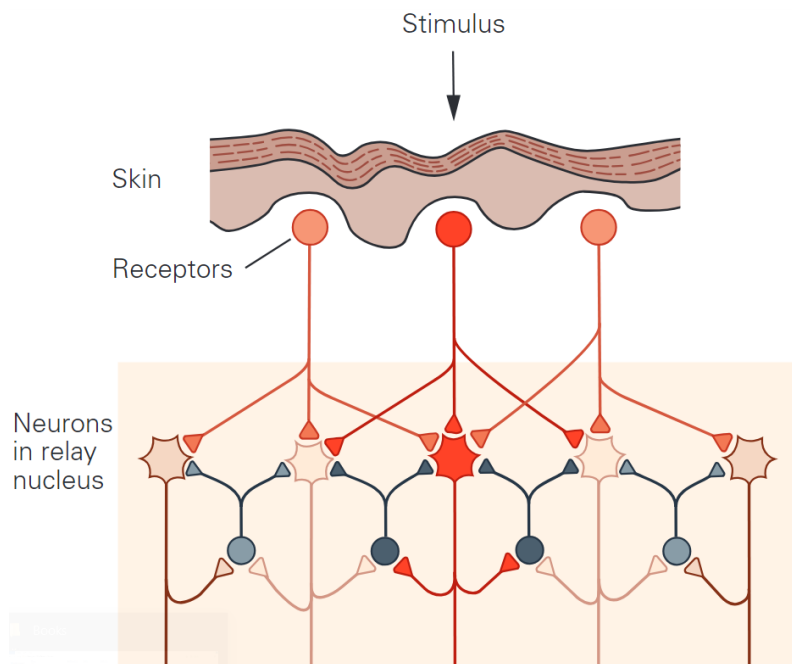


Figure E.2: Concept of lateral inhibition using feedback connections. [Kandel et al., 2013]

The lateral inhibition concept from Kandel et al. [2013] which is illustrated in Figure E.2 shows a stimulus which decays symmetrically as it is applied to the skin. The stimulus is relayed to neurons in the spinal cord, where the interneurons shown in black inhibit the stimulus laterally for each excitatory neuron. This concept served as the foundation for the model design in Figure E.3.

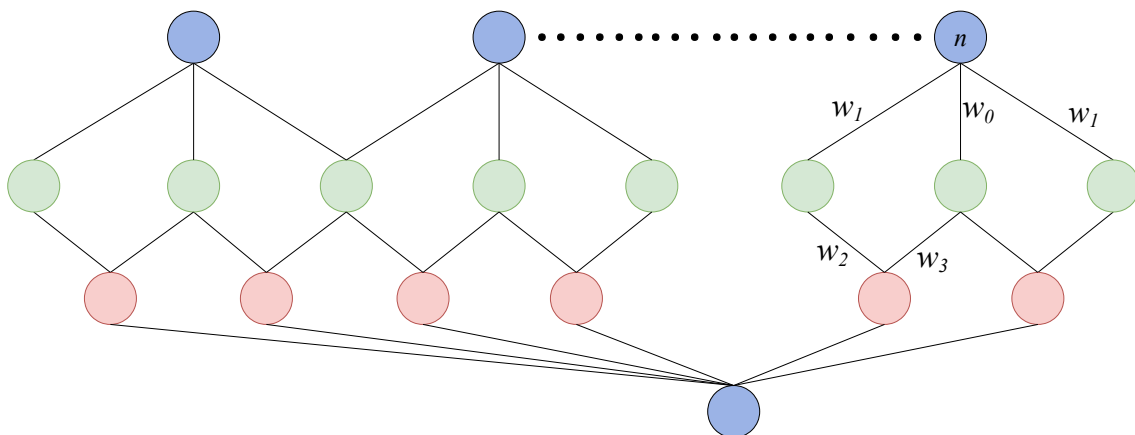


Figure E.3: The second design of the lateral inhibition model.

The network is a partially connected neural network with intended 12 nodes in the input layer. The input layer of this network is similar to the one presented in Figure E.1. The second layer represents interneurons and a third of the neurons in the entire network are thereby interneurons, which is a major difference between this design and the one

presented in Figure E.1. This was designed in order to make the network similar to the biology. However the concept in Figure E.2 also shows feedback connections which were not modelled in order to simplify the model. The output was designed to be the probability of distinguishing between one or two points. Similar to the first model the input represents stimuli applied to the skin. The weights w_0 and w_1 were chosen in order to achieve symmetrical decay from the stimulus center. The weights w_2 and w_3 were chosen to have negative values in order to implement lateral inhibition.